Study on the Circular Dichroism Measurements of Molecular Aggregates at Liquid-Liquid Interface

（液液界面分子集合体の円二色性測定に関する研究）

by

Hideaki Takechi

Department of Chemistry

Graduate School of Science

Osaka University

February, 2011

Contents

General Introduction

The self-assemblies of molecules into helical aggregates are ubiquitous in nature where they help, perform, and control all the important functions and processes of life.[1-5] This is hardly surprising considering that biological polymers are constructed of enantiomerically pure chiral units, the L-amino acids and D-sugars, leading proteins and nucleic acids to take on chiral secondary structures such as helical conformations. The key characteristic of chirality is enantiomeric specificity, which has an enormous impact on the pharmaceutical and material industries. For example, awareness of the differential effects of enantiomers on physiological processes (e.g. the tragedy of thalidomide) and, therefore, the necessity for single-enantiomer drugs have driven the development of critical chiral sysnthesis and purification of enantiometric drugs in industry.

Many researchers have used the process of a self-assembly as a model for the development of novel materials for use in diverse applications such as sensor, memory, lithography, and drug delivery.[6,7] In contrast to covalently bonded polymers and oligomers, the self-assembly is prodeced by non-covalent interactions, such as hydrophobic interaction, van der Waals and/or π-π stacking. It has been known that, under the right circumstances, chiral molecules assemble into helical aggregates whose topology reflects the underlying handedness of the individual constituents; that is, when the handedness of the molecules is reversed, the helicity of the aggregate also changes. The consequences of this for crystallization have been known since the time of Pasteur.[8,9] However, it is more recently that the importance of molecular chirality has been recognized in the case of self-assembled materials.

Optical rotary dispersion (ORD) and circular dichroism (CD) are now widely employed for characterizing and quantifying natural and synthetic chiral systems. Using a conventional circular dichroism spectropolarimeter, CD spectra have been measured not only for the isotropic samples, but also for various anisotropic samples such as solid, liquid crystal, film, membrane, micelles and gel. However, the CD spectra of anisotropic samples were more or less accompanied by artifacts due to the optical anisotropies of the samples, such as linear birefringence (LB) and linear dichroism (LD). Therefore, it is necessary to give a lot of care to such chiral artifacts in CD measurements, unless the samples are completely random-orientation systems such as solutions.[10,11]

The idea of a Mueller matrix measurement is not new. In 1978, R. M. A. Azzam and P. S. Hauge reported papers about Mueller matrix measurement.[12,13] Recently, transmission Mueller matrix ellipsometry, sometimes also referred so as to Mueller polarimetry, has been applied to the study of anisotropic samples with the intent of studying their optical activity. Interesting systems to study with this methodology correspond to samples containing oriented molecules[14] or to crystals[15-17]. In a similar way that, years ago, generalized ellipsometry and Mueller matrix ellipsometry started being used to measure anisotropic samples that could not be studied with standard ellipsometry, it seems reasonable to think that the future of polarimetric measurements of optical activity in anisotropic samples will rely on characteristics of the Mueller matrix. However, it is rare that Mueller matrix measurement is used for chiral anisotropic sample.[14,18] Because the magnitude of CD and CB effects is usually small. Moreover, in systems where linear birefringence and/or linear dichroism are also present they usually hinder the effect of CB and CD as they are orders of magnitude larger.

A liquid-liquid interface has been recognized not only as a boundary dividing two immiscible solvents, but also as a unique two-dimensional reaction field like a biomembrane.[19] The liquid/liquid interface offers functional potential for adsorbed molecules by the chemical manipulation of them. At the liquid/liquid interface, the molecules are highly mobile and rapidly achieve an equilibrium assembly. Studies on functional self-assembly systems having an highly-ordered structure at the liquid-liquid interface may be important not only to contribute to the understanding of a simple and/or essential mechanism for signal reception and transduction mimicking biological interfaces but also to provide the basis of a molecular device and/or a functional material capable of receiving and transferring information. Recently, we investigated the chiral aggregates of porphyrins and phthalocyanine formed at liquid/liquid interfaces. [20-22] However, the interfacial aggregation mechanism of porphyrin compounds are poorly understood.

The aim of the present study is to introduce the true chiral measurements at the liquid-liquid interface. Chapter 2 discussed the artifacts effects of circular dichroism signal at the liquid-liquid interface measured by the commercial CD spectrometer. We measured the correlations of CD and LD of liquid-liquid interfacial achiral ZnTPyP aggregates by the centrifugal liquid membrane (CLM) method and the home-built microscopic device, because LD is largest artifact parameter estimated from the calculation of Stokes vector and Mueller matrix.[10,11] In Chapter 3, H_4TPyP^{4+} and $CuTPPS^{4-}$ formed hetero-aggregates, which could recognize the chirality of D- and L- phenylalanines (Phe) and other amino acids at the liquid-liquid interface of the toluene-water system. The CD signal of the hetero-aggregates

was not artifact come from linear dichroism. Chapter 4 reported the Mueller matrix measurements at the liquid-liquid interfacial aggregates. The Mueller matrix description contains all the information about the polarization properties of a medium, and measurements of the complete Mueller matrix can be used to investigate the optical activity of a medium. This is the first report of Mueller matrix measurements at the liquid-liquid interface.

References

[1] J.D. Watson, F.H.C. Crick, *Nature*, **171**, 737 (1953).

[2] C.D. Tsai, B. Ma, S. Kumar, H. Wolfson, R. Nussinov, *Crit. Rev. Biochem. Mol. Biol.*, **36**, 399 (2001).

[3] K.-B. Scholthof, J. G. Shaw, M. Zaitlin, (Eds.) *Tobacco Mosaic Virus: One Hundred Years of Contributions to Virology*, Amer Phytopathological Society, Minnesota, 1999.

[4] V. Citovsky, *Phil. Trans. R. Soc. B*, **354**, 637 (1999).

[5] A. Klug, *Angew. Chem., Int. Ed.*, **22**, 565 (1983).

[6] D. D. Lasic, *Liposomes: From Physics to Applications.*, Elsevier, Amsterdam, 1993.

[7] J. M. Schnur, M. Peckerar, (Eds.) *Synthetic Microstructures in Biological Research.*, Plenum, New York, 1992.

[8] L. Pasteur, *Ann. Chim. Phys. (3rd Ser.)*, **28**, 56 (1850).

[9] Y. Tobe, *Mendeleev Commun.*, **2003**, 93.

[10] Y. Shindo, M. Nishio, S. Maeda, *Biopolymers*, **30**, 405 (1990).

[11] R. Kuroda, T. Harada, Y. Shindo, *Rev. Sci. Instrum.*, **72**, 3802 (2001).

[12] R. M. A. Azzam, *Opt. Lett.*, **2**, 148 (1978).

[13] P. S. Hauge, *J. Opt. Soc. Am.*, **68**, 1519 (1978).

[14] O. Arteaga, A. Canillas, R. Purrello, J. M. Ribó, *Opt. Lett.*, **34**, 2177 (2009).

[15] O. Arteaga, A. Canillas, J. Jellison, *Appl. Opt.*, **48**, 5307 (2009).

[16] B. Kahr, J. Freudenthal, E. Gunn, *Acc. Chem. Res.*, **43**, 684 (2010).

[17] J. H. Freudenthal, E. Hollis, B. Kahr, *Chirality*, **21**, S20 (2009).

[18] O. Arteaga, A. Canillas, J. Crusats, Z. El-Hachemi, J. Llorens, E. Sacristan, J. M. Ribó, *Chem. Phys. Chem.*, **11**, 3511 (2010).

[19] H. Watarai, N. Teramae, T. Sawada (Eds), *Interfacial Nanochemistry: Molecular Science and Engineering at Liquid-Liquid Interfaces (Nanostructure Science and Technology)*, Plenum Pub. Corp.: New York, USA, 2005.

[20] K. Adachi, K. Chayama, H. Watarai, *Langmuir*, **22**, 1630 (2006).

[21] H. Watarai, S. Wada, K. Fujiwara, *Tsinghua Science and Technology*, **11**, 228 (2006).

[22] K. Fujiwara, H. Monjushiro, H. Watarai, *Chem. Phys. Lett.*, **394**, 349 (2004).

Linear Dichroism of Zn(II)-tetrapyridylporphine Aggregates Formed at Toluene/Water Interface

Abstract

The apparent circular dichroism (CD) and the linear dichroism (LD) spectra of the aggregates of achiral zinc(II)-5,10,15,20-tetra(4-pyridyl)-21*H*,23*H*-porphine (ZnTPyP), formed at the toluene/water interface in a centrifugal liquid-membrane (CLM) cell, were investigated. It was confirmed that the apparent CD spectrum of ZnTPyP aggregates measured by CLM was the false signal come from the linear dichroism. The microscopic CD and LD spectra of the single interfacial aggregate of ZnTPyP with about 100 μm length were measured by a microscope-spectropolarimeter. It was suggested that the apparent CD spectrum of the single ZnTPyP aggregate measured by microscopic device was the artifacts come from a linear birefringence but not a linear dichroism. The interfacial ZnTPyP aggregate showed two types of flat trapezoidal shapes, one had a seed-like core at an edge (type I) and another a needle-like core at an edge (type II). Both of type I and type II structures showed two transition dipole moments, parallel and perpendicular to the long-axis of the structure, but suggesting a more developed J-aggregate in type II structure. AFM measurements showed that the interfacial ZnTPyP aggregate had multilayer structure, in which the unit monolayer thickness was 1.58 ± 0.23 nm.

Introduction

Self-aggregation and self-organization are natural processes caused mainly by noncovalent interactions, such as van der Waals, hydrogen bonding, hydrophilic/hydrophobic, electrostatic, donor and acceptor interactions, and coordination bonds.[1] As a "bottom-up" strategy, self-aggregation and self-organization are showing ever increasing importance in chemistry, material science, life science, and nanotechnology. Now, from natural and artificial self-assemblies, a wide variety of nanometer or micrometer sized structures and assemblies has been produced.[2-9] Advanced functions of self-assemblies may meet requirements of many objectives in industrial technology such as sensor, electronics, and electromechanical devices.[10-16]

Recently, the importance of molecular chirality in self-assembled materials has been extensively recognized. In living organisms, optically active macromolecules, such as proteins, nucleic acids, and polysaccharides, are universally involved in the life processes.[17,18] These macromolecules possess specific conformational and highly ordered structure associated with their chiral properties. In some cases, biological supramolecules exhibit a distinct helical or twisted structure, which is a conspicuous sign of the optical chirality of the supramolecular aggregate.[19-21] A variety of artificial self-assembled chiral structures have been synthesized from chiral molecules with noncovalent interactions, such as helical fiber and twisted ribbons of sugars,[22] helicenes,[23] helical metal complexes,[24-26] or block copolymers[27-29].

Optical rotary dispersion (ORD) and circular dichroism (CD) are now widely employed for characterizing and quantifying natural and synthetic chiral systems. Using a conventional circular dichroism spectropolarimeter, CD spectra have been measured not only for the isotropic samples, but also for various anisotropic samples such as solid, liquid crystal, film, membrane, micelles and gel. However, the CD spectra of anisotropic samples were more or less accompanied by artifacts due to the optical anisotropies of the samples, such as linear birefringence (LB) and linear dichroism (LD).[30] Therefore, it is necessary to give a lot of care to such chiral artifacts in CD measurements, unless the samples are completely random-orientation systems such as solutions.

Interfacial nanochemistry is growing as a new field in relation to analytical, separation, synthetic and molecular simulation sciences.[31] Determination of the structure of adsorbed species at the liquid-liquid interface is highly important in the study of kinetic mechanisms of solvent extraction and enzymatic reaction mechanisms at bio-membranes.[32] At the liquid-liquid interface, it is expected that a molecular aggregate, which is not formed in the bulk phase, can be formed easily, because the interfacial concentration of a surface active monomer

becomes much higher than that in the bulk phase. The adsorption and aggregation behaviors of molecules were investigated by means of various methods.[33-37] Recently, we investigated the chiral aggregates of porphyrins and phthalocyanine formed at liquid/liquid interfaces by circular dichroism measurements combined with a centrifugal liquid-membrane (CLM) technique or a second-harmonic generation spectrometry (SHG).[38-40] It has been suggested by a CLM-CD measurement that the interfacial self-aggregate of zinc(II)-5,10,15,20-tetra(4-pyridyl)-21*H*,23*H*-porphine (ZnTPyP) shows an apparent circular dichroism.[41] In the present study, the cause of the apparent circular dichroism of ZnTPyP aggregates reported previously[41] was investigated in detail from the comparison between the CD and LD spectra measured by CLM method and those measured by a new microscopic spectropolarimeter technique. The present method, which examines the correlation between the CD and LD spectra, is thought to be very useful as a criterion of the genuine optical chirality, since a simple linear relationship will be observed in the case of an achiral and anisotropic system. Furthermore, the characteristic structure of the interfacial self-aggregate of ZnTPyP was examined by optical microscope and AFM measurements. In the present study, the orientation analysis of the interfacial aggregates in the CLM cell has also been carried out for the first time.

Experimental

Materials.

Zinc(II)-5,10,15,20-tetra(4-pyridyl)-21*H*,23*H*-porphine (ZnTPyP, Figure 1), and sodium perchlorate (GR grade) were purchased from Aldrich (USA). Toluene and chloroform (GR grade) were purchased from Nacalai Tesque Inc. (Kyoto, Japan) and used as received. Toluene was a poor solvent for ZnTPyP. Therefore, toluene including 5% chloroform was used as the organic phase solvent. Chloroform was also used to prepare the stock solution of ZnTPyP. Water was distilled and deionized by a Milli-Q system (Millipore, USA).

UV-Vis Absorption, Linear Dichroism and Circular Dichroism Spectral Measurements by Centrifugal Liquid-Membrane (CLM) Technique.

The formation of self-aggregate of ZnTPyP at the toluene/water interface was directly observed using the CLM-Abs, CLM-LD and CLM-CD methods,[43,44] in which the CLM cell was installed in the CD spectropolarimeter (J-820E, JASCO, Japan). The apparatus for the CLM-Abs and CLM-CD measurements were essentially the same with the one reported

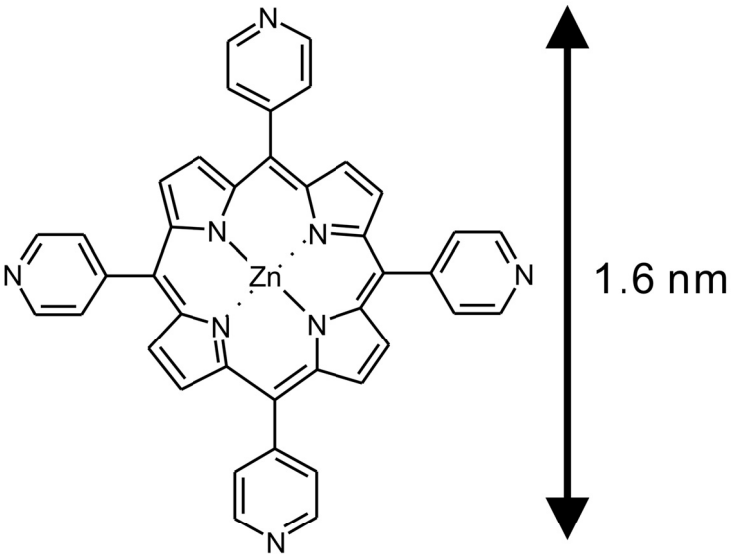

Figure 1. Molecular structure of ZnTPyP. The size of ZnTPyP is the reported size of TPyP, which is a ZnTPyP analogue compound.[42]

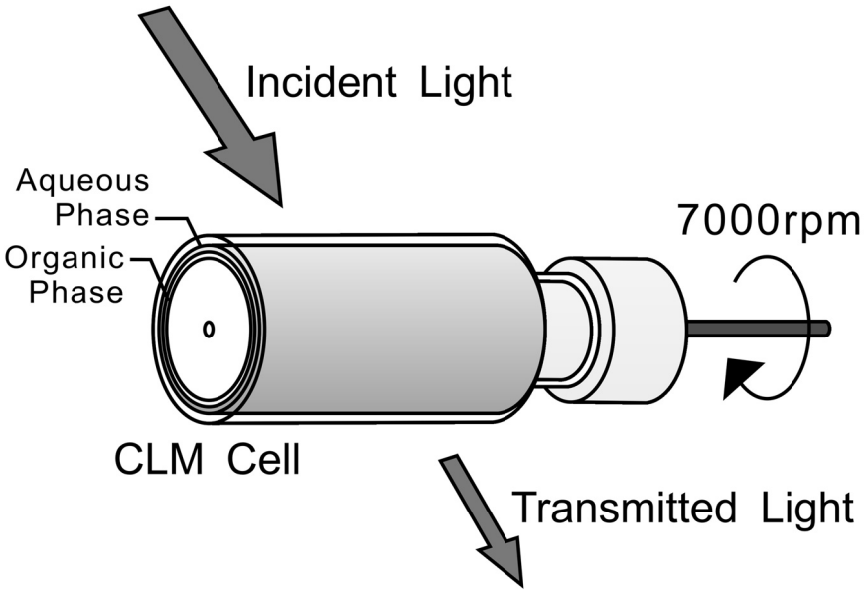

Figure 2. Schematic illustration of CLM method.

previously,[44] but CLM-LD method was introduced in the present sturdy. Figure 2 shows the outline of the CLM method. A cylindrical cell, whose height and outer diameter were 3.4 cm and 1.9 cm, respectively, was placed horizontally in the sample chamber of the polarimeter and rotated at 7000 rpm by a speed-controlled electric motor (NE-22E, Nakanishi Inc., Japan). At first, a blank spectrum was measured by introducing 0.500 mL of an aqueous solution of 0.1M $NaClO_4$ (pH5.5) and 0.380 mL toluene with a microsyringe into the cylindrical cell. Then, 0.020 mL of a chloroform solution of ZnTPyP was added and the interfacial reaction was initiated. The sum of the spectra of the bulk phase and the interface was measured by this

method. The calculated values of the thickness of the organic and aqueous phase were 0.20 and 0.25 mm, respectively. The interfacial area, S_i, between two phases was 20 cm^2.

Microscopic UV-Vis Absorption, Linear Dichroism and Circular Dichroism Measurements of a Single Interfacial Aggregate.

We employed the home-built microscopic device, which was installed in a sample chamber of the CD spectropolarimeter (J-820, JASCO, Japan). The detail of this method was reported previously.[45] Figure 3 shows the schematic illustration of the microscopic spectropolarimeter. Briefly, the circularly polarized beam or the linear polarized beam from a light source of the polarimeter was condensed to the sample on a cover glass, which was vertically fixed on a position-orientation controllable stage, through an object lens (20×), and the penetrated beam was expanded again by an another objective lens (20×), and then detected by a frequency control technique to obtain CD, LD and UV/Vis spectra of a minute region (60 μm × 20 μm) of the sample. The measurement region and the rotation angle of the sample were checked by CCD images through the same objective lens. The blank spectra were got from no sample region of the cover glass. The aggregate formed at the liquid/liquid interface was transferred on a cover glass by a simple lifting method.

AFM Measurement.

The AFM images of the ZnTPyP aggregates transferred on a cover glass after CLM measurement were measured by an atomic force microscope SPI3800N/SPA400 (SII NanoTechnology Inc., Tokyo, Japan) with a silicon cantilever, using the tapping mode. AFM images were presented in the height mode without any image processing except flattening.

Other Apparatus.

The pH value of the aqueous phase was measured by a F-14 pH meter (HORIBA, Japan) equipped with a 6366-10D glass electrode. To observe the image of ZnTPyP aggregates at the liquid/liquid interface by a conventional optical microscope, a flat interface was required under the objective. For this purpose, we used a two-phase glass cell reported previously, which was constructed by an outer glass cylinder cell (41 mm i.d. and 8.0 mm height) and an inner glass cylinder (36 mm i.d. and 5.0 mm in height).[46]

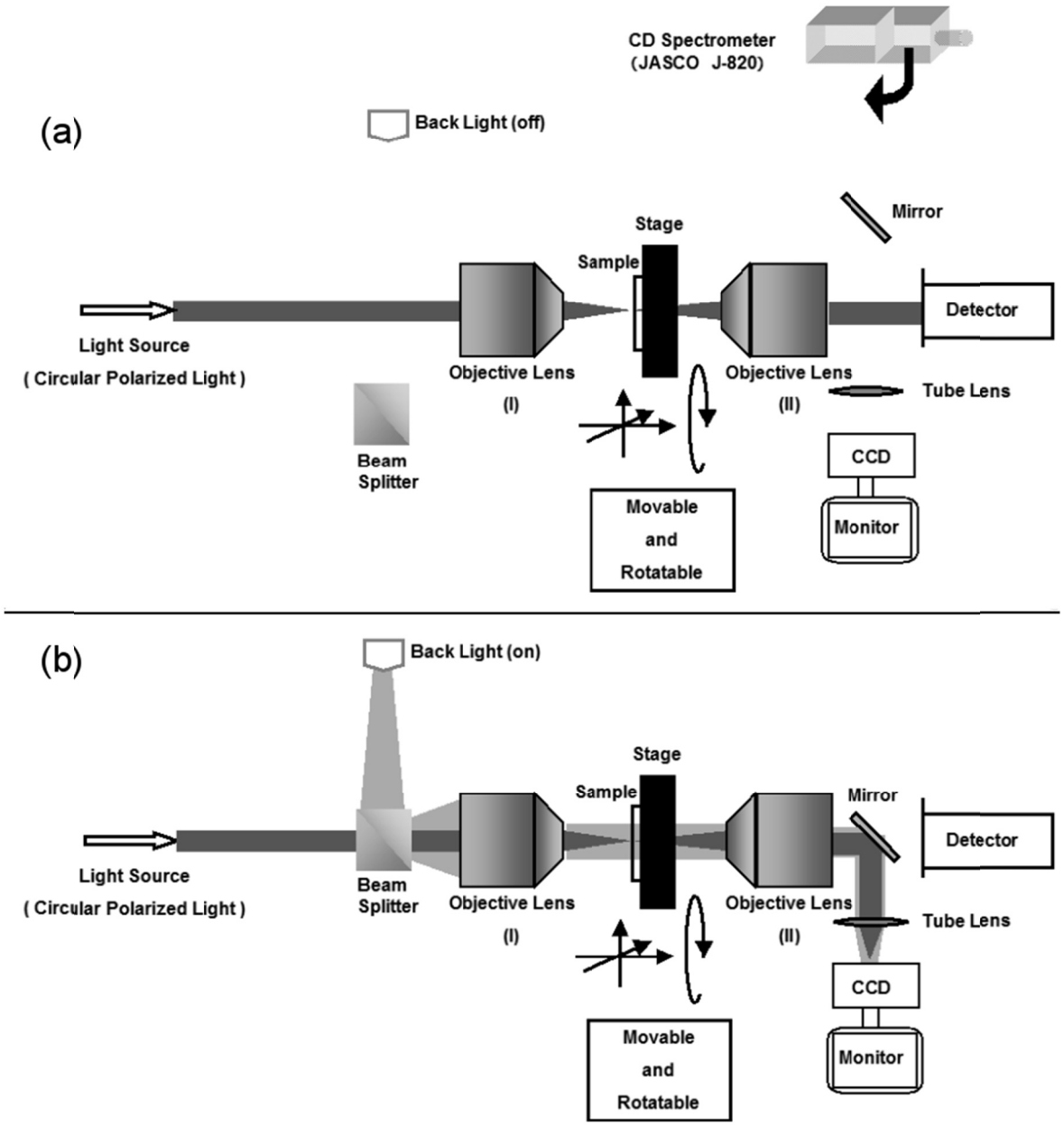

Figure 3. Schematic illustration of the microscopic spectropolarimeter. (a) Set up for a measurement and (b) Set up for observing sample images by CCD.

Results and Discussion

Interfacial Self-Aggregation of ZnTPyP at the Toluene/Water System.

The interfacial self-aggregation of ZnTPyP at the toluene/water system was directly measured using the centrifugal liquid–membrane-absorption spectrometry (CLM-Abs)[43], the centrifugal liquid-membrane-circular dichroism spectroscopy (CLM-CD)[44] and the centrifugal liquid-membrane-linear dichroism spectroscopy (CLM-LD). The preliminary study on the process of the interfacial self-aggregation of ZnTPyP has been reported previously.[47] It reported that ZnTPyP was highly interfacial active and formed self-aggregates by the bonding between zinc and the pyridyl group at the liquid-liquid interface. The previous results of CLM measurements showed that ZnTPyP monomer peak at 423 nm gradually decrease with time, while a new peak at 454 nm assigned to ZnTPyP aggregate appeared and reached an equilibrium after about 8 min under the conditions of 7.5×10^{-6} M ZnTPyP in the organic phase (toluene/chloroform = 95/5, v/v) and 0.1 M $NaClO_4$ in the aqueous phase. In the present study, CLM spectra of ZnTPyP aggregates were obtained at 30 min later after the start of the reaction.

CLM-Abs, CLM-CD and CLM-LD spectra of ZnTPyP aggregates are shown in Figure 4. The CLM-Abs spectrum shows a new peak at 454 nm, which is not observed in ZnTPyP monomer solution, thus assignable to ZnTPyP aggregates formed at the liquid/liquid interface. Though the CD spectrum of ZnTPyP monomer solution showed no optical chirality, the CLM-CD spectrum gave an apparent optical chirality, should be due to the interfacial ZnTPyP aggregates.[41] In the present study, the observed CLM-CD spectrum of the aggregate looked like a mirror image of the CLM-LD spectrum. Therefore, we thought that the circular dichroism reported previously was mainly due to the large linear dichroism. We confirmed whether the CD spectrum came from the LD spectrum quantitatively.

Kuroda *et al.* reported CD signal (CD_{app}) and LD signal (LD_{app}) measured by commercial CD spectrometer can be expressed as,[30]

$$\begin{aligned}
\mathrm{CD}_{\mathrm{app}} = {} & G_1(P_x^2 + P_y^2)[\mathrm{CD} + 1/2(\mathrm{LD}'\,\mathrm{LB} - \mathrm{LD}\,\mathrm{LB}') + (\mathrm{LD}'\sin 2\theta - \mathrm{LD}\cos 2\theta)\sin\alpha] \\
& + G_1(P_x^2 - P_y^2)\sin 2a\{-\mathrm{LB}\cos 2\theta + \mathrm{LB}'\sin 2\theta \\
& + [-\mathrm{CB} + 1/2(\mathrm{LD}^2 + \mathrm{LB}^2 - \mathrm{LD}'^2 - \mathrm{LB}'^2)\sin 4\theta \\
& + (\mathrm{LD}'\,\mathrm{LD} + \mathrm{LB}'\,\mathrm{LB})\cos 4\theta]\sin\alpha\} \qquad (1), \\
& + G_1(P_x^2 - P_y^2)\cos 2a\{\mathrm{LB}'\cos 2\theta - \mathrm{LB}\sin 2\theta \\
& + [1 + 1/2(\mathrm{LD}'^2 - \mathrm{LB}^2)\sin^2 2\theta + 1/2(\mathrm{LD}^2 - \mathrm{LB}'^2)\cos^2 2\theta \\
& - 2(\mathrm{LD}'\,\mathrm{LD} + \mathrm{LB}'\,\mathrm{LB})\sin 4\theta]\sin\alpha\}
\end{aligned}$$

$$\begin{aligned}\mathrm{LD}_{\mathrm{app}} &= G_2(P_x^2 + P_y^2)\{\mathrm{LD}'\sin 2\theta - \mathrm{LD}\cos 2\theta + [\mathrm{CD} + 1/2(\mathrm{LD}'\,\mathrm{LB} - \mathrm{LD}\,\mathrm{LB}')]\sin\alpha\} \\ &+ G_2(P_x^2 - P_y^2)\sin 2a\{-\mathrm{CB} + 1/2(\mathrm{LD}^2 + \mathrm{LB}^2 - \mathrm{LD}'^2 - \mathrm{LB}'^2)\sin 4\theta \\ &+ (\mathrm{LD}'\,\mathrm{LD} + \mathrm{LB}'\,\mathrm{LB})\cos 4\theta + (\mathrm{LB}'\sin 2\theta - \mathrm{LB}\cos 2\theta)\sin\alpha\} \\ &+ G_2(P_x^2 - P_y^2)\cos 2a[1 + 1/2(\mathrm{LD}'^2 - \mathrm{LB}^2)\sin^2 2\theta \\ &+ 1/2(\mathrm{LD}^2 - \mathrm{LB}'^2)\cos^2 2\theta - 2(\mathrm{LD}'\,\mathrm{LD} + \mathrm{LB}'\,\mathrm{LB})\sin 4\theta \\ &+ (\mathrm{LB}'\cos 2\theta - \mathrm{LB}\sin 2\theta)\sin\alpha]\end{aligned} \quad (2).$$

Here, CB, LD, LD', LB, and LB' are circular birefringence, (x-y) linear dichroism, 45° linear dichroism, (x-y) linear birefringence, and 45° birefringence, respectively. P_x^2 and P_y^2 are the transmittance of the photomultiplier along the x and y directions and "*a*" is the azimuth angle of its optical axis with respect to the x axis. θ is the rotation angle of the sample, and α is the residual static birefringence of the photoelastic modulator (PEM). G_1 and G_2 are the apparatus constant related to the sensitivity of the spectrometer at 50 kHz and 100 kHz, respectively. Eqs (1), (2) can be approximated as,[30,48]

$$\begin{aligned}\mathrm{CD}_{\mathrm{app}} &= G_1(P_x^2 + P_y^2)[\mathrm{CD} + 1/2(\mathrm{LD}'\,\mathrm{LB} - \mathrm{LD}\,\mathrm{LB}') + (\mathrm{LD}'\sin 2\theta - \mathrm{LD}\cos 2\theta)\sin\alpha] \\ &+ G_1(P_x^2 - P_y^2)\sin 2a(-\mathrm{LB}\cos 2\theta + \mathrm{LB}'\sin 2\theta) \\ &+ G_1(P_x^2 - P_y^2)\cos 2a(\mathrm{LB}'\cos 2\theta - \mathrm{LB}\sin 2\theta)\end{aligned} \quad (3),$$

$$\begin{aligned}\mathrm{LD}_{\mathrm{app}} &= G_2(P_x^2 + P_y^2)(\mathrm{LD}'\sin 2\theta - \mathrm{LD}\cos 2\theta) \\ &+ G_2(P_x^2 - P_y^2)\sin 2a\{-\mathrm{CB} + 1/2(\mathrm{LD}^2 + \mathrm{LB}^2 - \mathrm{LD}'^2 - \mathrm{LB}'^2)\sin 4\theta \\ &+ (\mathrm{LD}'\,\mathrm{LD} + \mathrm{LB}'\,\mathrm{LB})\cos 4\theta\}\end{aligned} \quad (4).$$

Because the CD spectrometer was calibrated, we considered $G_1(P_x^2 + P_y^2) = 1$ and $G_2(P_x^2 + P_y^2) = 1$. To simplify the analysis, we regarded Eq. (4) as,

$$\mathrm{LD}_{\mathrm{app}} = \mathrm{LD}'\sin 2\theta - \mathrm{LD}\cos 2\theta \quad (5).$$

And, sin α of the CD spectrometer in our laboratory was -5.4×10^{-3} (at 449.5 nm) determined by the polarizer, that has only LD and LD', and Eq. (3). This sin α value was the same order to the sin $\alpha = -7.1 \times 10^{-3}$ (at 250 nm) reported previously.[49] At first, we checked the third term contribution of Eq. (3), (LD' sin 2θ – LD cos 2θ) sin α. In Figure 5, the solid line show (LD' sin 2θ – LD cos 2θ) sin α calculated by $\mathrm{LD}_{\mathrm{app}}$ spectrum of Figure 4 and the above sin $\alpha = -5.4 \times 10^{-3}$. The solid line corresponded to the dotted line of $\mathrm{CD}_{\mathrm{app}}$ spectrum. Therefore, we can conclude that the apparent CD spectrum of ZnTPyP interfacial self-aggregate was the artifact, mainly due to the LD spectrum.

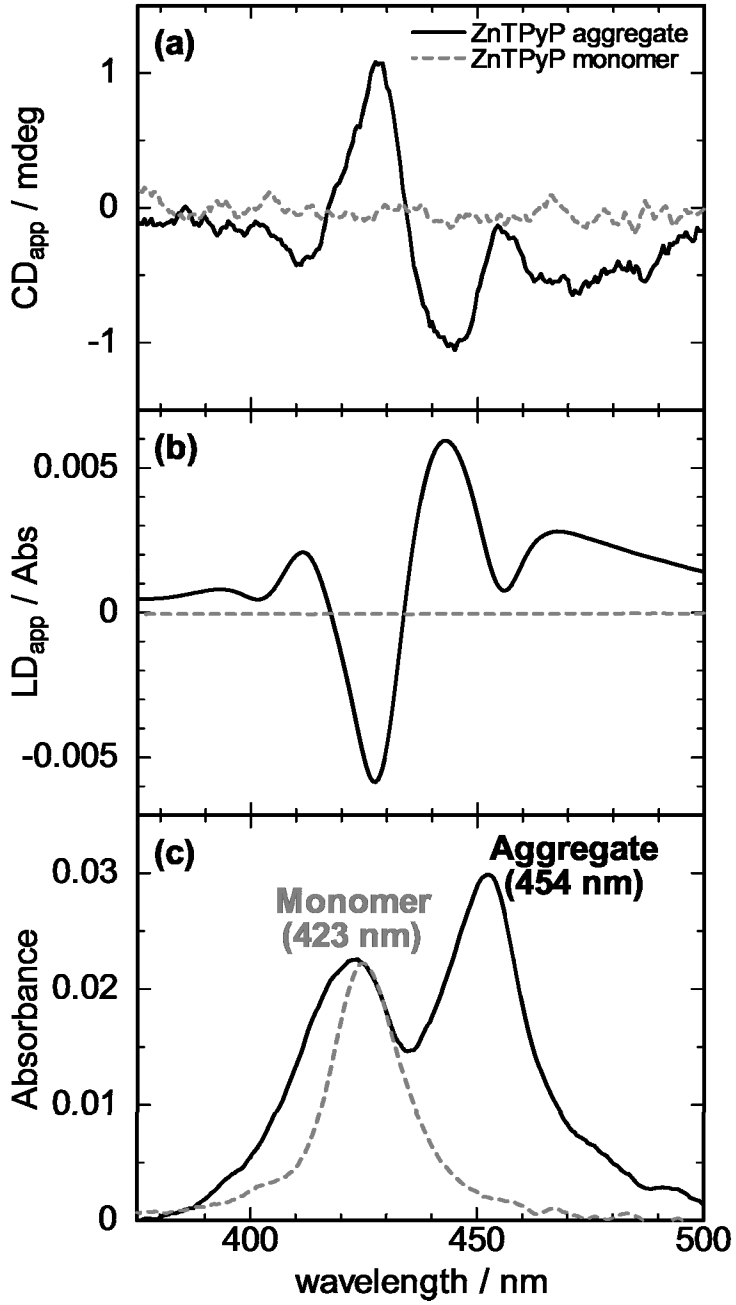

Figure 4. (a) Circular dichroism (CD) spectra, (b) linear dichroism (LD) spectra and (c) absorption spectra of ZnTPyP aggregates in the toluene/water system measured by the CLM method (solid line) and ZnTPyP monomer solution in 1 mm cell (dashed line). The concentration of ZnTPyP in the organic phase (toluene/chloroform = 95/5, v/v) in a CLM cell was 7.5×10^{-6} M (solid line) and the concentration of ZnTPyP solution (toluene/chloroform = 95/5, v/v) in a 1 mm cell was 8.9×10^{-7} M (dashed line).

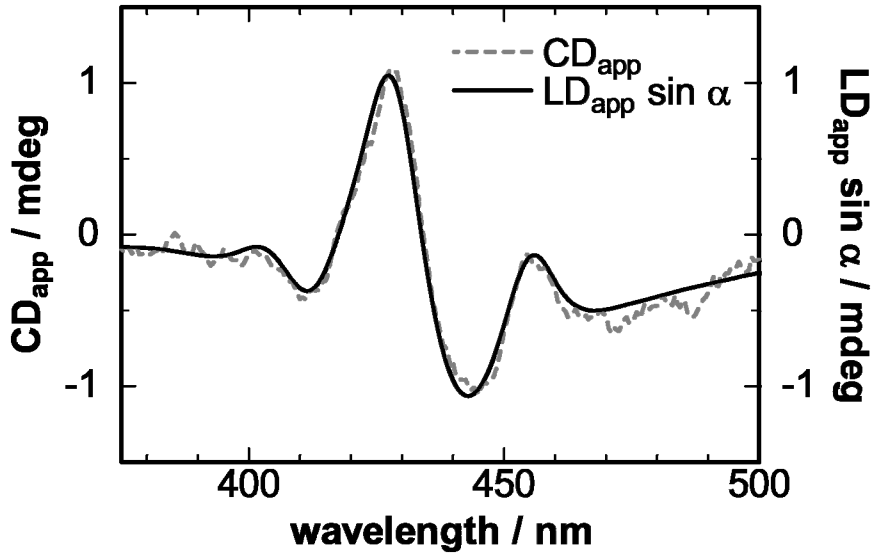

Figure 5. LD_{app} sin α contribution in CD spectrum of Figure 4 (b).

Linear Dichroism Spectra of a Single ZnTPyP Aggregate.

To discuss the orientational structure of ZnTPyP interfacial self-aggregate, we measured CD and LD spectra of an individual ZnTPyP aggregate by applying the new microscopic CD measurement device. ZnTPyP aggregates formed at the interface of CLM cell were rather small in size, giving only a few micrometers, when observed after the CLM measurements. Therefore, it was difficult to measure the microscopic CD or LD spectrum of an individual ZnTPyP aggregate by defining the orientation angle of the single aggregate. To make larger ZnTPyP aggregates, we used a two-phase glass cell, whose liquid/liquid interface was flat and whose specific interface area was 1.0 cm^{-1}. Figure 6 is the optical microscopic images of ZnTPyP aggregates formed at the liquid/liquid interface of the two-phase glass cell under the initial concentration of $[ZnTPyP]_{ini} = 4.0 \times 10^{-6}$ M. The interfacial aggregates had mainly flat and trapezoidal structure, different from the ZnTPyP crystals formed in a bulk solution that had thicker trapezoidal structure. Each semitransparent ZnTPyP aggregate at the interface had a black seed structure at the edge of the aggregate or a dark needle structure in an edge of the aggregate. We called them a seed-type (type I) and a needle-type (type II), respectively. To find any difference between type I and type II aggregates, CD and LD spectra of a single ZnTPyP aggregate were measured by the microspectropolarimeter.

ZnTPyP aggregate was transferred form the interface on a cover glass and fixed on the movable and rotatable stage to obtain CD and LD spectra by the microspectropolarimeter with the various angles of θ, which was defined as the angle between a long-axis of the vertical rectangular beam and the long-axis of ZnTPyP aggregate (Figure 7). Measurements were done for the type I ZnTPyP aggregate (Figure 8 (a)) and the type II ZnTPyP aggregate (Figure 8 (b)).

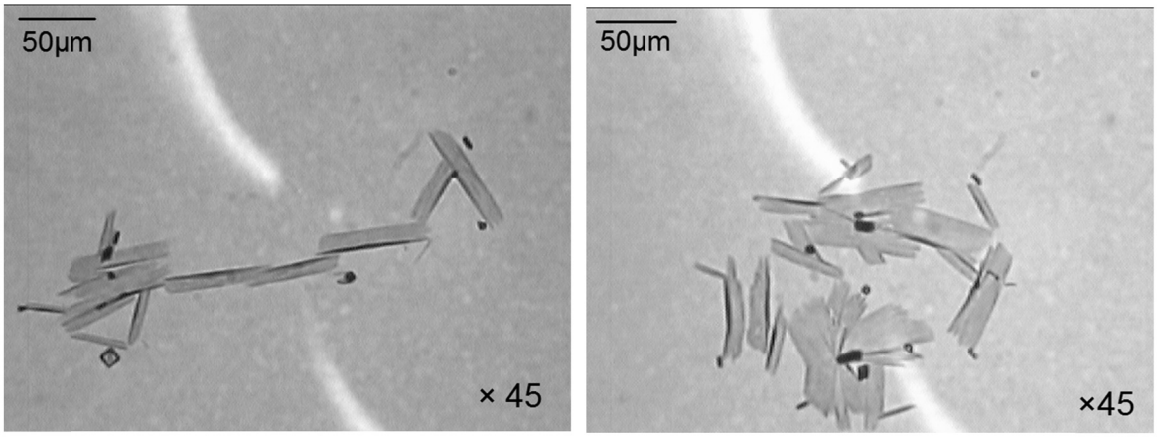

Figure 6. Typical optical microscopic images of self-aggregates of ZnTPyP at the liquid-liquid interface. Each structure has a seed-like core at a center (type I) or needle-like core at an edge (type II). The concentration of ZnTPyP in the organic phase (toluene/chloroform = 95/5, v/v) was 4.0×10^{-6} M in the two-phase system. The concentration of $NaClO_4$ in the aqueous phase was 0.1 M (pH = 5.5).

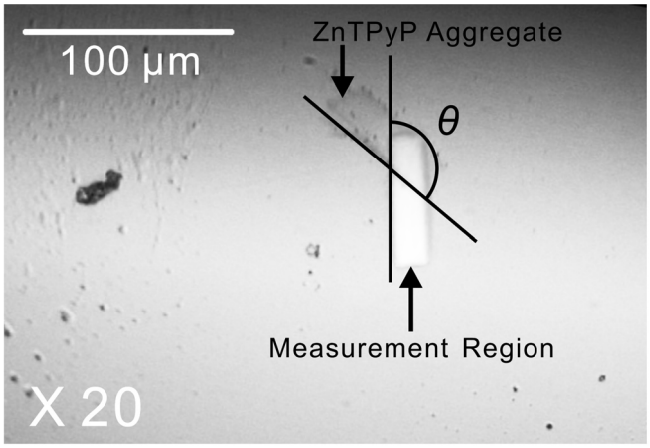

Figure 7. CCD image of a ZnTPyP aggregate taken by a microscopic devise. Here, θ is angle between the polarized light and a long-axis of a ZnTPyP aggregate.

The observed micro-LD, micro-CD and micro-Abs spectra of an individual structure of type I and type II aggregates are shown in Figure 8 (c) and (d), respectively. The absorption spectra of the type I aggregates had two maxima at about 420nm and 450nm, though the 420 nm peak was smaller than the 450 nm peak. While in the absorption spectrum of type II aggregate, the intensities at the maxima at 420 nm and 460 nm were almost same. Miyake *et al.* reported that ZnTPyP monolayer at the air/water interface had a similar absorption spectrum showing a smaller maximum at 422 nm and a larger maximum at 466 nm, suggesting an overlapped aggregate structure.[50] But they didn't discuss the possibility of the interaction between pyridyl nitrogen and Zn(II) ion. In the micro-LD and micro-CD spectra, the difference between type I and type II is more remarkable. The maximum at 450 nm in type I shifted to 470 nm in type II aggregate as noted from Figure 8 (c) and (d), suggesting more extended J-aggregation in type II.

Thus, it was noted that the extent of the J-aggregation of ZnTPyP molecules in the aggregate depended on the structures of the dark portion in the aggregate; seed-type and needle-type.

The observed LD intensity is defined by the absorbance at a horizontally polarized light minus the absorbance at a vertically polarized light. If a ZnTPyP aggregate has only one transition dipole parallel to the long-axis of a trapezoidal aggregate, the LD intensity should have maximum at $\theta = 90$ °, minimum at $\theta = 0$ ° and 180 ° and zero at $\theta = 45$ ° and 135 °. However, the observed LD spectra were different from this simple prediction as shown in Figure 8 (c) and (d). In the LD spectra of type I aggregate (Figure 8 (c)), the LD intensities were in the order of LD ($\theta = 90$ °) > LD ($\theta = 135$ °) > LD ($\theta = 180$ °) at 450 nm and 410 nm. However, at 430 nm, the order was completely reversed. However, at 430 nm, the order was completely reversed. This result indicates that the electric transition dipole moments corresponding to the maxima at 450 nm and 410 nm are parallel to the long-axis of the aggregate and that corresponding to 430 nm is perpendicular to the long-axis (Figure 9) in type I structure. On the other hand, the transition dipole moments of type II aggregate at 470 nm, 440 nm and 400 nm are parallel to the long-axis, and that at 430 nm is perpendicular to the long-axis.

Here, LD sign of single ZnTPyP aggregate directed to parallel was similar to LD spectrum of ZnTPyP aggregates measured by CLM. So, it was indicated that the long axis of the aggregate at the interface in the CLM cell have orientated to the rotating axis of the CLM cell.

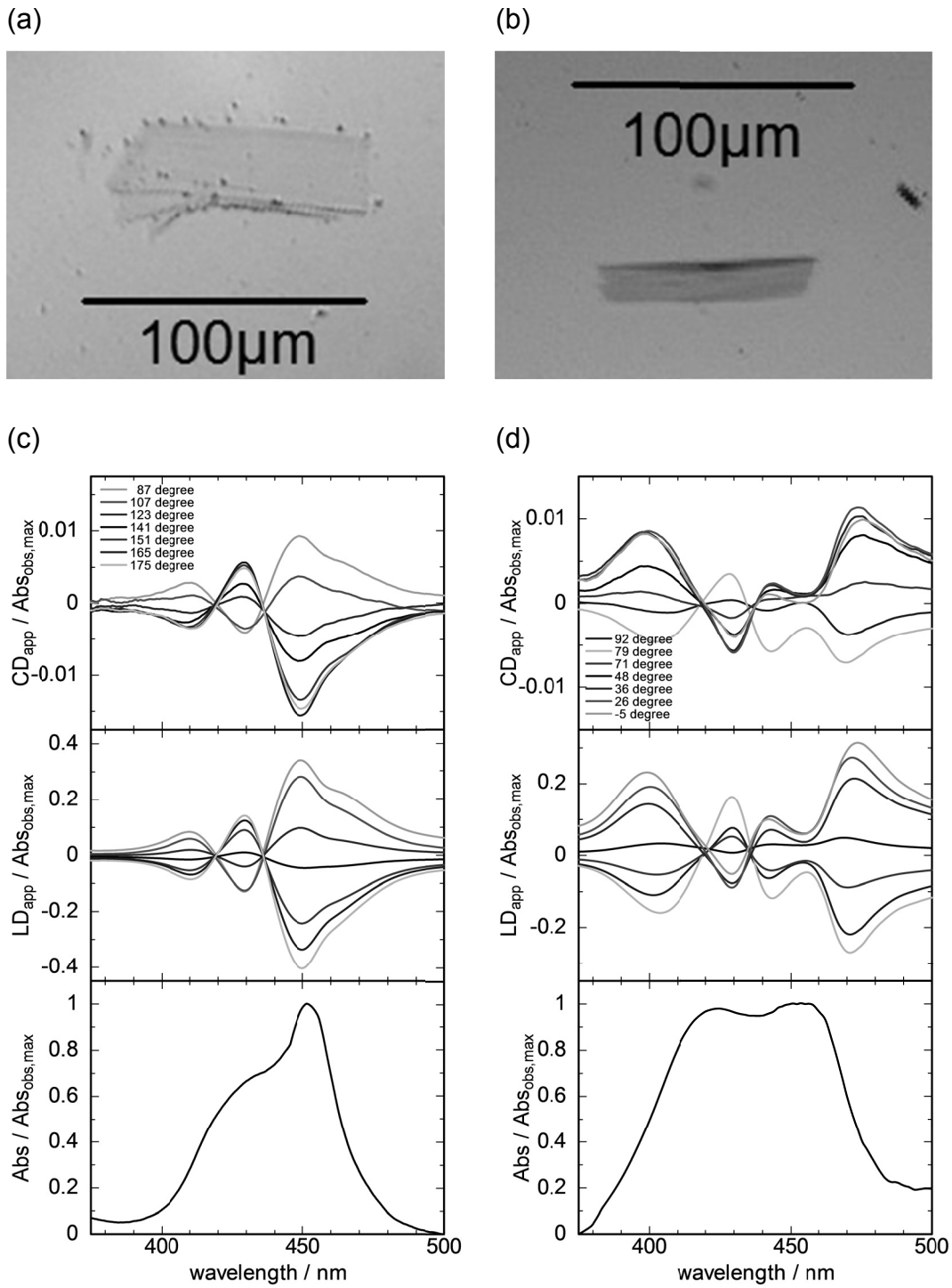

Figure 8. CCD images of a type I of ZnTPyP aggregate which has a seed-like core (a) and a type II of ZnTPyP aggregate which has a needle-like core (b). LD, CD and absorption spectra of the type I ZnTPyP aggregate (c) and the type II ZnTPyP aggregate (d) were measured by a microscopic spectropolarimeter. These spectra were normalized at the absorption maximum. CD and LD spectra were measured at various angles, and θ values are noted in the figure.

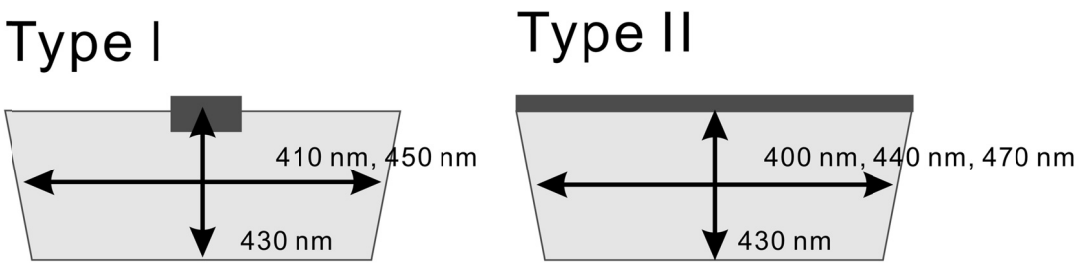

Figure 8. Illustrations of ZnTPyP aggregate which had a seed (Type I) and a needle (Type II) at the edge of the aggregates. Arrows show the directions of electric transition dipole moments in ZnTPyP aggregate suggested by micro-LD measurements.

Correlation between Micro-LD and Micro-CD Spectra.

The CD spectrum of ZnTPyP aggregate measured by CLM was the artifacts mainly came from the LD spectrum. We investigated whether the micro-CD spectra of the ZnTPyP aggregate was also the artifacts due to the LD spectrum or not.

In Figure 8 (c) and (d), the shape of the micro-LD and micro-CD spectra at various angles of θ for type I and type II aggregates were very similar, though the maximum wavelengths were different between type I and type II. The dependence of micro-LD and apparent micro-CD intensities on the angle θ at 449.5 nm was examined for a type I aggregate (Figure 9 (a)).

Figure 9 (b) shows the correlation between micro-LD and micro-CD intensities of type I aggregate at 449.5 nm. The θ values were changed from 0 to 180 degree by selecting properly oriented aggregate. Figure 9 (b) shows a elliptical correlation between LD_{app} and CD_{app} intensities, suggesting a significant relationship between LD_{app} and CD_{app} of ZnTPyP aggregate. Similar correlation between LD_{app} and CD_{app} intensities was also observed for type II aggregate (Figure 8 (d)), although the figure was not shown. In Figure 9 (b), the solid line showed LD_{app} sin α in Eq. (3). The apparent CD of the type I aggregate could not be fitted by the LD_{app} sin α. In Figure 9 (c), the dotted line also showed LD sin α in Eq. (3). The apparent CD of the angle dependence of type I aggregate also could not be fitted by LD sin α. So, micro-CD of the ZnTPyP aggregate was not the artifacts due to the LD. But the micro-CD showed the angle dependence with 180 º cycle, so the apparent CD was not chiral signal. In Eq. (3), the term responsible to the 180 º cycle dependence is LB term except for LD sin α. Here, $G_1(P_x^2 - P_y^2)$ = 0.049 (at 220 nm) was reported previously.[48] To simplify the analysis, we regarded a = 0. The solid line of Figure 9 (c) was the fitted one by LB term in Eq. (3). LB = –0.16 and LB' = –0.26 were determined from this fitting. Kuroda *et al.* reported that a sample with macroscopic

anisotropy like crystal, e.g., α-$Ni(H_2O)_6SO_4$, had not only a large LD signal, but also a large LB signal.[30] So, it is not strange that ZnTPyP aggregate had both LD and LB. Therefore, the origin of the apparent micro-CD of ZnTPyP aggregate was assigned mainly to the LB term in Eq. (3).

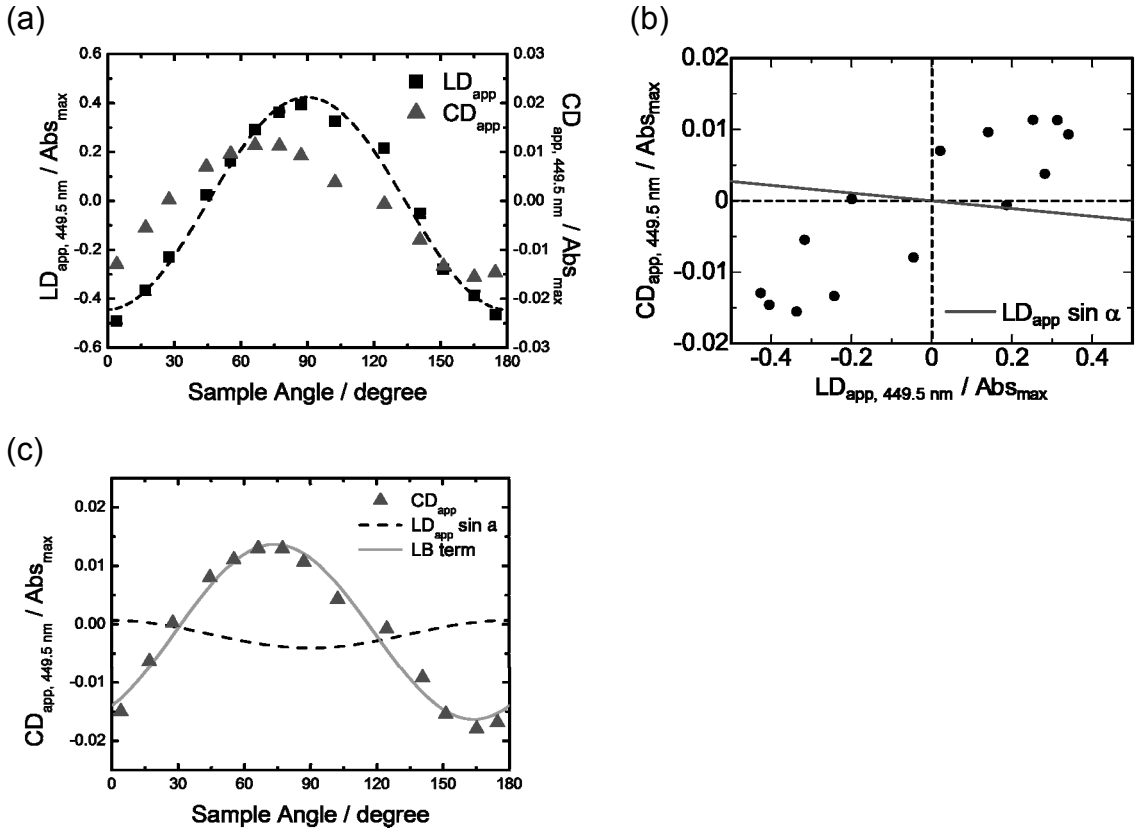

Figure 9. (a) CD and LD intensities of the type I of ZnTPyP aggregate (Figure 7 (b)) at the 449.5 nm measured by the microscopic spectropolarimeter, when the angle between the polarized vertical light and a long-axis of a ZnTPyP aggregate, θ, was changed. CD and LD values were normalized at the absorption maximum. The dashed lines was fitted by Eq. (5). (b) Correlation between CD and LD intensities at various θ angles. The solid line is the LD_{app} sin α term in Eq. (3). (c) The dashed line shows LD_{app} sin α in Eq. (3) contribution in CD intensity of type I aggregate at 449.5 nm. The solid line is fitted by LB term in Eq. (3).

Nano-structure of ZnTPyP Aggregate.

We tried to get further structural information of the interfacial self-aggregate of ZnTPyP, but the aggregates were too small to measure X-ray diffraction patterns. Instead, the aggregates were transferred onto a cover glass and observed by AFM. Figure 10 (a) shows the AFM image of ZnTPyP aggregate, which is a part of the corner of the rectangular structure assignable to a type II aggregate. The thickness of the flat region of the aggregate was about 10 nm, and that of the needle-like region of the edge was about 40 nm. Such very thin structure of ZnTPyP aggregates might be ascribable to a few nanometer-thickness of the liquid/liquid interfacial region.[52] The needle-like portion at an edge of an aggregate observed by an optical microscope was confirmed to be thicker than the flat region. The flat region of the aggregate had nano-steps as shown in Figure 10 (b). The Gaussian analysis of the observed steps was shown in Figure 10 (c). The peaks of Gaussian fit were appeared at 1.58 ± 0.23 nm, 3.08 ± 0.13 nm and 4.60 ± 0.37 nm, giving the constant interval of about 1.6 nm. Therefore, the thickness of the unit step was obtained as 1.58 ± 0.23 nm from the first Gaussian peak. Interestingly, the unit thickness is almost the same size with a ZnTPyP molecule presented in Figure 1. This indicates that the unit step is a monolayer of ZnTPyP molecules, in which the ZnTPyP molecules are assembled stood perpendicularly.

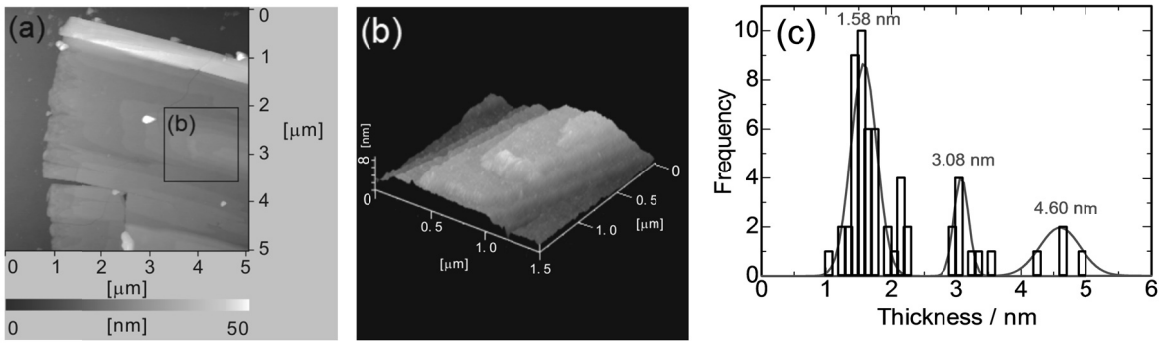

Figure 10. (a) The AFM image of the interfacial self-aggregate of ZnTPyP (Type II) after a CLM measurement ($[ZnTPyP]_{ini}$ = 2.5 × 10^{-6} M), transferred on a cover glass. (b) 3D image of the flat region of the ZnTPyP aggregate. (c) Distribution of the thickness of the step of the flat region of ZnTPyP aggregate.

Conclusion

The CD and LD measurements of the interfacial ZnTPyP aggregates using the CLM method revealed that the apparent CD of the ZnTPyP aggregates reported previously was mainly due to the linear dichroism.[41] But apparent CD spectrum of a single ZnTPyP aggregate measured by microscopic device introduced in CD spectrometer was the artifacts come from a linear birefringence but not a linear dichroism. From the comparison between the CLM-LD and micro-LD measurements, it was indicated that the interfacial aggregate formed in the CLM cell could be orientated nearly parallel to the rotating axis of the CLM cell. The individual ZnTPyP aggregate had two types of structure; a seed-type (type I) and a needle-type (type II), which are relating to the characteristic LD spectra. Both type I and type II ZnTPyP aggregates had electric transition dipole moments of two directions, parallel and perpendicular to long-axis of the ZnTPyP aggregate. J-coupling of ZnTPyP molecular transition dipole moments was seemed pronounced more in the type II along with the long-axis of the trapezoidal structure. The thickness of unit monolayer of ZnTPyP aggregate was estimated as 1.58 ± 0.23 nm from the AFM measurements. From the present results, the molecular image of the micro-structure of ZnTPyP aggregate was thought to be a stacked monolayers of ZnTPyP molecules, which was composed by the coordination bond between zinc(II) and pyridyl nitrogen and the van der Waals stacking between porphyrin rings.[8,53] A molecular origin of the differences between type I and type II aggregates is still obscure. However, it is plausible that ZnTPyP aggregate at the liquid-liquid interface, which is a border of two solvents, had some different structures, because Goldberg *et al.* reported the different structures of ZnTPyP crystals were produced depending on the molecules included, such as water, methanol, aniline, and o-chlorophenol, by X-ray diffraction measurements.[53,54] We have demonstrated in the present study that the apparent CD spectrum of interfacial aggregates could be expressed with Eq. (3). When the CD spectrum of interfacial aggregates is measured by the CD spectrometer, it is necessary to give a lot of care to artifacts come from linear anisotropy like a linear dichroism and a linear birefringence.

References

[1] G. M. Whitesides, B. Grzybowski, *Science*, **295**, 2418 (2002).

[2] L. F. Zhang, K. Yu, A. Eisenberg, *Science*, **272**, 1777 (1996).

[3] D. E. Discher, A. Eisenberg, *Science*, **297**, 967 (2002).

[4] P. X. Gao, Y. Ding, W. Mai, W. L. Hughes, C. S. Lao, Z. L. Wang, *Science*, **309**, 1700 (2005).

[5] X. Y. Kong, Y. Ding, R. S. Yang, Z. L. Wang, *Science*, **303**, 1348 (2004).

[6] T. Kato, *Science*, **295**, 2414 (2002).

[7] T. Shimizu, M. Masuda, H. Minamikawa, *Chem. Rev.*, **105**, 1401 (2005).

[8] J. S. Hu, Y. G. Guo, H. P. Liang, L. J. Wan, L. Jiang, *J. Am. Chem. Soc.*, **127**, 17090 (2005).

[9] H. Liu, Q. Zhao, Y. Li, Y. Liu, F. Lu, J. Zhuang, S. Wang, L. Jiang, D. Zhu, D. Yu, L. Chi, *J. Am. Chem. Soc.*, **127**, 1120 (2005).

[10] C. M. Drain, *Proc. Natl. Acad. Sci. U.S.A.*, **99**, 5178 (2002).

[11] C. Du, G. Falini, S. Fermani, C. Abbott, J. Moradian-Oldak, *Science*, **307**, 1450 (2005).

[12] D. G. Kurth, P. Lehmann, M. Schütte, *Proc. Natl. Acad. Sci. U.S.A.*, **97**, 5704 (2000).

[13] S. Park, J. H. Lim, S. W. Chung, C. A. Mirkin, *Science*, **303,** 348 (2004).

[14] E. Winfree, F. Liu, L. A. Wenzler, N. C. Seeman, *Nature*, **394**, 539 (1998).

[15] D. M. Vriezema, M. C. Aragonès, J. A. A. W. Elemans, J. J. L. M. Cornelissen, A. E. Rowan, R. J. M. Nolte, *Chem. Rev.*, **105**, 1445 (2005).

[16] H. Cölfen, S. Mann, *Angew. Chem. Int. Ed.*, **42**, 2350 (2003).

[17] J. D. Watson, F. H. C. Crick, *Nature*, **171**, 737 (1953).

[18] J. P. Straley, *Phys. Rev. A*, **14**, 1835 (1976).

[19] D. M. Engelman, T. A. Steitz, *Cell*, **23**, 411 (1981).

[20] D. Eisenberg, R. M. Weiss, T. C. Terwilliger, *Nature*, **299**, 371 (1982).

[21] P. W. Hildebrand, K. Rother, A. Goede, R. Preissner, C. Frömmel, *Biophys. J.*, **88**, 1970 (2005).

[22] J. H. Fuhrhop, W. Helfrich, *Chem. Rev.*, **93**, 1565 (1993).

[23] C. Nuckolls, T. J. Katz, T. Verbiest, S. V. Elshocht, H. G. Kuball, S. Kiesewalter, A. J. Lovinger, A. Persoons, *J. Am. Chem. Soc.*, **120**, 8656 (1998).

[24] S. Shinoda, T. Okazaki,T. N. Player, H. Misaki, K. Hori, H. Tsukube, *J. Org. Chem.*, **70**, 1835 (2005).

[25] Z. Wu, G. Yang, Q. Chen, J. Liu, S. Yang, J. S. Ma, *Inorg. Chem. Comm.*, *7*, 249 (2004).

[26] T. Kawamoto, B. S. Hammes, B. Haggerty, G. P. A. Yap, A. L. Rheingold, A. S. Borovik, *J. Am. Chem. Soc.*, **118**, 285 (1996).

[27] K. Morino, M. Oobo, E. Yashima, *Macromolecules*, **38**, 3461 (2005).

[28] H. Goto, H. Q. Zhang, E. Yashima, *J. Am. Chem. Soc.*, **125**, 2516 (2003).

[29] R. Nonokawa, E. Yashima, *J. Am. Chem. Soc.*, **125**, 1278 (2003).

[30] R. Kuroda, T. Harada, Y. Shindo, *Rev. Sci. Instrum.*, **72**, 3802 (2001).

[31] H. Watarai, N. Teramae, T. Sawada, (Eds.) *Interfacial Nanochemistry: Molecular Science and Engineering at Liquid-Liquid Interfaces (Nanostructure Science and Technology)*; Plenum: New York, 2005.

[32] A. G. Volkov, (Eds.) *Liquid Interfaces in Chemical, Biological and Pharmaceutical Applications*; Marcel Dekker: New York, 1997.

[33] K. Fujiwara, H. Monjushiro, H. Watarai, *Rev. Sci. Instrum.*, **76**, 023111 (2005).

[34] Y. Yulizar, H. Monjushiro, H. Watarai, *J. Colloid Interface Sci.*, **275**, 560 (2004).

[35] W. H. Steel, F. Damkaci, R. Nolan, R. A. Walker, *J. Am. Chem. Soc.*, **124**, 4824 (2002).

[36] H. Nagatani, Z. Samec, P. F. Brevet,D. J. Fermin, H. H. Girault, *J. Phys. Chem. B*, **107**, 786 (2003).

[37] Y. Moriya, S. Nakata, H. Morimoto, N. Ogawa, *Anal. Sci*., **20**, 1533 (2004).

[38] K. Adachi, K. Chayama, H. Watarai, *Langmuir*, *22*, 1630 (2006).

[39] H. Watarai, S. Wada, K. Fujiwara, *Tsinghua Science and Technology*, **11**, 228 (2006).

[40] K. Fujiwara, H. Monjushiro, H. Watarai, *Chem. Phys. Lett.*, **394**, 349 (2004).

[41] Y. Matsumoto, H. Watarai, *Solv. Extr. Res. Dev. Jpn.*, **13**, 207 (2006).

[42] C. V. K.Sharma, G. A. Broker, G. J. Szulczewski, R. D. Rogers, *Chem. Commun*., **2000**, 1023.

[43] H. Nagatani, H. Watarai, *Anal. Chem*., **70**, 2860 (1998).

[44] S. Wada, K. Fujiwara, H. Monjushiro, H. Watarai, *Anal. Sci.*, **20**, 1489 (2004).

[45] A. Matsugaki, H. Takechi, H. Monjushiro, H. Watarai**,** *Anal. Sci.*, **24**, 297-300 (2008).

[46] S. Yamamoto, H. Watarai, *Langmuir*, **22**, 6562 (2006).

[47] H. Takechi, H. Watarai, *Solv. Extr. Res. Dev. Jpn.*, **14**, 133 (2007).

[48] Y. Shindo, M. Nishio, S. Maeda, *Biopolymers*, **30**, 405 (1990).

[49] T. Harada, T. Sato, R. Kuroda, *Chem. Phys. Lett.*, **413**, 445 (2005).

[50] D. J. Qian, C. Nakamura, J. Miyake, *Langmuir*, **16**, 9615 (2000).

[51] Y. Shino, Y. Ohmi, *J. Am. Chem. Soc.*, **107**, 91 (1985).

[52] H. Watarai, M. Gotoh, N. Gotoh, *Bull. Chem. Soc. Jpn.*, **70**, 957 (1997).

[53] H. Krupitsky, Z. Stein, I. Goldberg, C. E. Strouse, *J. Inclusion Phenom.*, **18**, 177 (1994).

[53] S. George, I. Goldberg, *Acta Cryst.*, **E61**, m1441 (2005).

Chiral Recognition of Amino-Acids by Synergistic Hetero-Aggregation with Porphyrins at Liquid-Liquid Interface

Abstract

At the interface of the toluene/water system, H_4TPyP^{4+} and $CuTPPS^{4-}$ formed hetero-aggregates, which could recognize the chirality of D- and L- phenylalanines (Phe) and other amino acids, though neither H_4TPyP^{4+} nor $CuTPPS^{4-}$ could recognize the chirality of the amino-acids. The composition of H_4TPyP^{4+}: $CuTPPS^{4-}$ in the interfacial aggregate was estimated as 1:1 as reported in an aqueous solution. But, CD spectra of the interfacial hetero-aggregates were different from that in the aqueous solution, suggesting different chiral structure. The present result proposed a new mode of the interfacial chiral recognition reaction exhibited by the synergistic effect of the hetero-aggregation of the inversely charged porphyrins.

Introduction

The liquid-liquid interface has some attractive functions such as the selective concentration of surface active species from bulk phases and the isothermal adsorption relationship, like Langmuir equation, in the interfacial adsorption. A two dimensional concentrated mono-molecular layer is ready to be generated at the interface with the saturation concentration in the order of 10^{-10} mol cm^{-2}. Therefore, at the liquid-liquid interface, supramolecular aggregates tend to be formed even under a low bulk concentration of the monomer. These features of liquid-liquid interfaces are thought to be advantageous for the chiral analysis of bulk phase species, combined with an effective technique to observe optical chirality at the interface. Recently, in our laboratory, a centrifugal liquid-membrane-circular dichroism (CLM-CD) and a second-harmonic generation-circular dichroism (SHG-CD) methods were developed, and the chiral aggregation of porphyrins and phthalocyanines formed at liquid-liquid interfaces were investigated.[1-3] However, the promising potential of the interfacial aggregation for the chiral analysis has not been fully understood. Purrello *et al*. have reported that protonated form (H_4TPyP^{4+}, Figure 1) of 5,10,15,20-tetra(4-pyridyl)-21*H*,23*H*-porphine (TPyP, Figure 1), deprotpnated form ($CuTPPS^{4-}$, Figure 1) of Cu(II)- meso-tetra(4-sulfonatophenyl) porphine (CuTPPS, Figure 1) and phenylalanine formed chiral hetero-aggregates in acidic aqueous solutions showing an induced circular dichroism (ICD),[4] though the reaction mechanism was not clarified. In the present study, the feasibility of H_4TPyP^{4+}-$CuTPPS^{4-}$ hetero-aggregates for the chiral recognition of amino acids at the liquid-liquid interface has been demonstrated by using CLM-CD method. TPyP was dissolved in an organic phase, and $CuTPPS^{4-}$ and phenylalanine were dissolved in an acid aqueous phase (pH 2.3) at first.

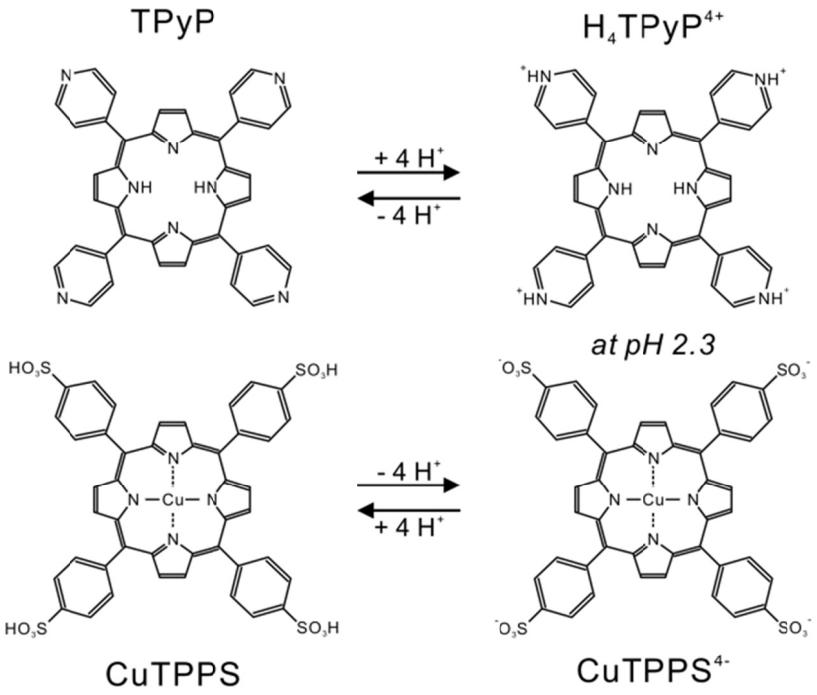

Figure 1. Molecular structures of TPyP and CuTPPS.

Experimental

Materials.

CuTPPS was purchased from Frontier Scientific, Inc. (USA). TPyP and sodium perchlorate were purchased from Aldrich (USA). D-Phenylalanine (D-Phe) and D, L-tyrosine were purchased from Wako (Osaka, Japan). L-Phenylalanine (L-Phe), D, L-tryptophan, perchloric acid, toluene and chloroform were purchased from Nacalai Tesque Inc. (Kyoto, Japan) and used as received. Toluene was a poor solvent for TPyP. Therefore, toluene containing 4 % chloroform was used as the organic phase solvent. Chloroform was also used to prepare the stock solution of TPyP. Water was distilled and deionized by a Milli-Q system (Millipore, USA).

UV-Vis Absorption, Linear Dichroism and Circular Dichroism Spectral Measurements by Centrifugal Liquid-Membrane (CLM) Technique.

The formation of chiral hetero-aggregates of H_4TPyP^{4+}, $CuTPPS^{4-}$ and phenylalanine at the toluene/water system was directly measured using the centrifugal liquid membrane-absorption spectrometry (CLM-Abs),[5] the centrifugal liquid membrane-circular dichroism spectroscopy (CLM-CD),[6,7] and the centrifugal liquid membrane-linear dichroism

spectroscopy (CLM-LD).[7] In the CLM measurements, a cylindrical glass cell, having 1.9 cm in diameter and 3.4 cm in length, was placed horizontally, attached by an electric motor in the sample chamber of the CD spectropolarimeter (J-820E, JASCO, Japan). The procedure for the CLM measurements was essentially the same with Chapter 2. The cylindrical cell was rotated at 7000 rpm by a speed-controlled electric motor (NE-22E, Nakanishi Inc., Japan). At first, a blank spectrum was measured by introducing 0.480 mL of an aqueous solution of 0 - 0.05 M phenylalanine and 0.1 M (H^+, Na^+) ClO_4^- (pH 2.3) and 0.480 mL toluene with a microsyringe into the cylindrical cell through a sample injection hole. Then, 0.020 mL of aqueous solution of $CuTPPS^{4-}$ and 0.020 mL of a chloroform solution of TPyP were added to initiate the interfacial reaction. The sum of the spectra of the bulk liquid membrane phases and the interface was measured by this method. The calculated values of the thickness of the organic and aqueous phase were 0.26 and 0.25 mm, respectively. The interfacial area between two phases was 20 cm^2.

Interfacial Tension Mesurements.

The interfacial tension at the toluene/water (20.8 mL/8.0 mL) interface was measured using the Wilhelmy balance technique with a 10.0 × 10.0 mm filter paper plate.[8] An interfacial pressure sensor (USI-32, Hybrid Instruments Co., Japan) was used, interfaced to a digital meter. The accuracy of the measurements was ±0.1 mN/m. It was always confirmed that the interfacial tension attained its ‘‘equilibrium value,’’ which did not vary by more than 0.2 mN/m over a period of 15 min. In some cases, it took more than 1 h. All the measurements were conducted at 27 ± 2 ºC, using a UC-65 cryostat (EYELA, Japan). In the interfacial tension experiments, H_4TPyP^{4+} stock solution was prepared in an acidic solution of pH 2.3. The pH values of the aqueous phases were measured using a F-14 pH meter (HORIBA, Japan) equipped with a 6366-10D glass electrode.

The relationship between γ and the concentration of a sample in the aqueous phase, c_{aq}, could be expressed with the next equation, [9,10]

$$\gamma = \gamma_0 - aRT \ln\left(1 + \frac{c_{aq} K'}{a}\right) \quad (1),$$

where γ_0, R, T and a are the interfacial tension in the absence of the sample, the gas constant, the absolute temperature, and the interfacial saturated concentration, respectively, and the interfacial adsorption constant at the infinite dilution of the sample, K’, can be written as,

$$K' = \frac{c_i}{c_{aq}} \quad (2),$$

where c_i is the interfacial concentration.

Results and Discussion

Chiral Recognition by TPyP-CuTPPS Hetero-Aggregates.

Figure 2 shows the CLM-CD spectra of the H_4TPyP^{4+}-$CuTPPS^{4-}$ chiral hetero-aggregates including D- and L-Phe, which had three maxima at ca. 400 nm, 410 nm and 450 nm (small) indicating the chirality of added amino-acid. The formation rate of the chiral hetero-aggregates observed by the CLM-CD spectra depended remarkably on the concentrations of TPyP, $CuTPPS^{4-}$ and phenylalanine. The CD intensity increased continuously with time at first, then saturated, and began to decrease finally, suggesting agglomeration of the aggregate. In the shortest case, the saturation time was ca. 30 min. In the conditions of Figure 2, the saturation time was ca. 6 hr. In Figure 2, the CD intensity at 30 min was used for the composition analysis of the aggregate to avoid the slow agglomeration of the aggregate.

After the CLM-CD measurement, any CD signal was not observed in the organic phase and about 2 % of the CLM-CD intensity was observed in the aqueous phase, but it was negligible. Hence, it was concluded that the CD signal observed by the CLM measurements came from the interface.

The sign of the CD spectra of H_4TPyP^{4+}-$CuTPPS^{4-}$hetero-aggregates at the liquid-liquid interface reversed depending on the chirality of D-phenylalanine and L-phenylalanine, and there was no CD signal in the racemic phenylalanine solution as shown in Figure 2. A linear correlation between the CD intensity at 410 nm and the chiral excess of phenylalanine was confirmed as shown in Figure 4. The observed fitted linear line of the induced CD intensity was CD = –28.7 e.e., where e.e. was defined by e.e. = ([D-Phe] - [L-Phe]) /([D-Phe] + [L-Phe]). This relationship can be used for the determination of the chiral purity of the phenylalanine, under the conditions of [Phe] = 9.6×10^{-3} M and t = 30 min. In Chapter 2, it was problem that the interfacial CLM-CD signal contained the false signal which came from the linear anisotropy of the interfacial aggregate like linear dichroism (LD). Therefore, we measured CLM-LD spectra of H_4TPyP^{4+}-$CuTPPS^{4-}$ hetero-aggregates in the present study. However, the LD intensity was weak and there was no correlation between CD and LD intensities. Thus, CD signals of the present interfacial hetero-aggregates were thought to be really chiral signals. This section demonstrated that TPyP-CuTPPS hetero-aggregates could recognize the chirality of phenylalnine, we mainly used D-phenylalnine in the experiment of the section after this.

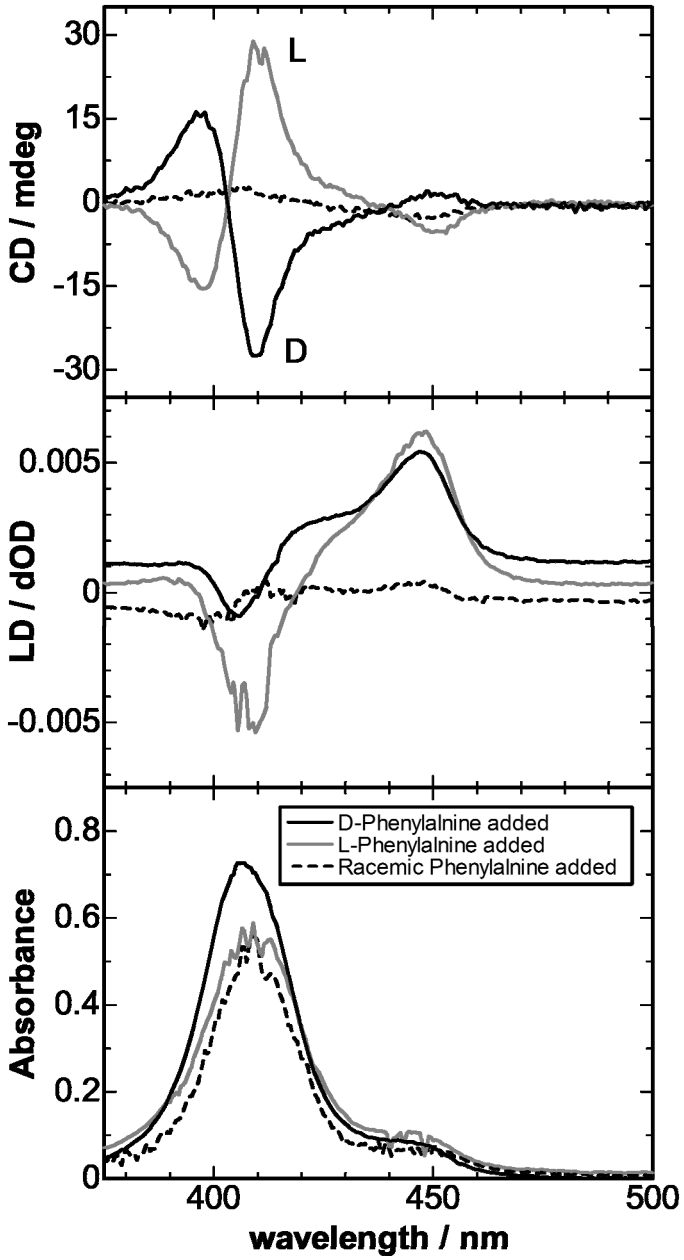

Figure 2. CD, LD and absorbance spectra of chiral hetero-aggregates at the liquid-liquid interface measured by CLM-CD. $[TPyP]_{org}$ = 8.0 × 10^{-6} M, $[CuTPPS^{4-}]_{aq}$ = 7.2 × 10^{-5} M, $[Phe]_{aq}$ = 9.6 × 10^{-3} M, $[HClO_4]_{aq}$ + $[NaClO_4]_{aq}$ = 0.1 M, pH 2.3, Toluene:Chloroform = 96:4, v/v, t = 30 min.

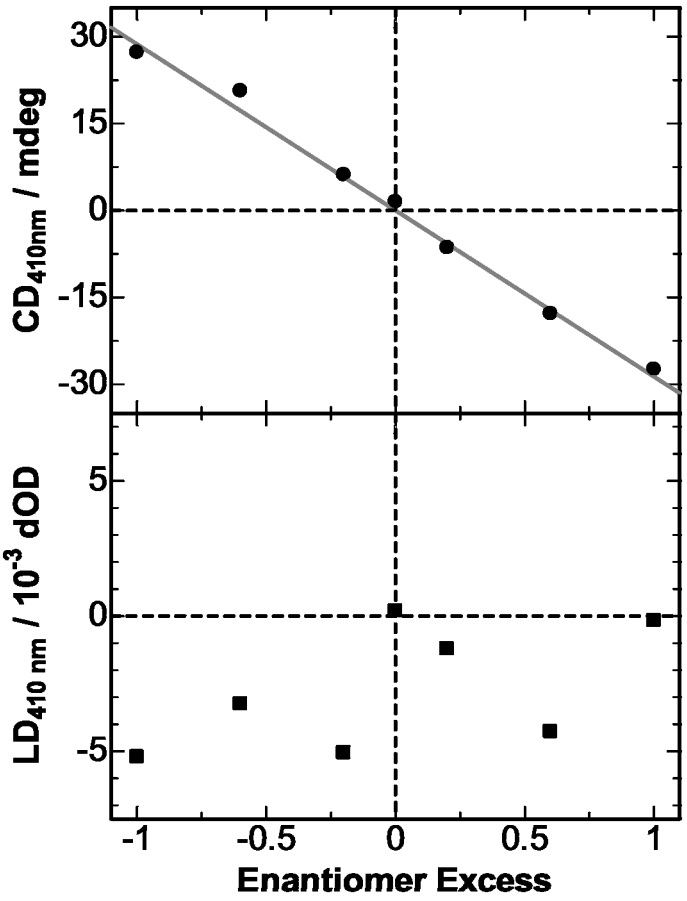

Figure 3. Correlations of enantiomer excess of phenylalanine, e.e. = ([D-Phe] - [L-Phe]) /([D-Phe] + [L-Phe]), and CD, LD signals of TPyP-CuTPPS hetero-aggregates measured by CLM-CD. The linear solid line is a fitted line by the linear function that goes through the origin. $[TPyP]_{org}$ = 8.0 × 10^{-6} M, $[CuTPPS]_{aq}$ = 7.2 × 10^{-5} M, $[Phe]_{aq}$ = 9.6 × 10^{-3} M, $[HClO_4]_{aq}$ + $[NaClO_4]_{aq}$ = 0.1 M, pH 2.3, toluene:chloroform = 96:4, v/v, t = 30 min.

Influence of Liquid-Liquid Interfacial Adsorption

Circle plots of Figure 4 show the Job plot of H_4TPyP^{4+}-$CuTPPS^{4-}$ hetero-aggregate in the toluene/water system. Figure 5 shows the concentration dependence of CD intensity of TPyP-CuTPPS hetero-aggregates in the toluene/water system. Circle plots of Figure 4 and Figure 5 indicated that, only when all components of H_4TPyP^{4+}, $CuTPPS^{4-}$ and phenylalanine exist in the toluene/water system, CD signal of hetero-aggregates could be observed. Furthermore, CD signal appeared, when all TPyP, CuTPPS and phenylalnine concentrations were larger than the critical concentrations of $[TPyP]_c$, $[CuTPPS]_c$ and $[Phe]_c$. The critical concentrations were summarized in Table 1. The critical concentrations were different among the chemical species greatly. Here, we thought that this difference comes from the difference of the liquid-liquid interfacial adsorptivity. The interfacial tension of toluene/water systems including H_4TPyP^{4+}, $CuTPPS^{4-}$ and phenylalanine was observed by the Wilhelmy plate method to evaluate the adsorptivity of these reactants.

The results of interfacial tension measurements were shown in Figure 6. The above critical concentration was larger than the concentration that the interfacial tension begun to decrease. So, it was suggested that these chemical species exist in the liquid-liquid interface at the critical concentration. Interfacial adsorption constants from the aqueous phase to the liquid-liquid interface were determined by Eq. (1) and summarized in Table 1. The interfacial adsorption constants decreased in the order of H_4TPyP^{4+} > $CuTPPS^{4-}$ >> phenylalanine. When the interfacial adsorption constant is large, the critical concentration seems to be small. Figure 4 shows that chiral hetero-aggregate was difficult to be generated, when the concentration of one chemical species was very high. So, it was thought that H_4TPyP^{4+}, $CuTPPS^{4-}$ and phenylalanine adsorbed competitively to the liquid-liquid interface and the chiral hetero-aggregates could be formed when the interfacial concentrations of H_4TPyP^{4+}, $CuTPPS^{4-}$ and phenylalanine were almost same order.

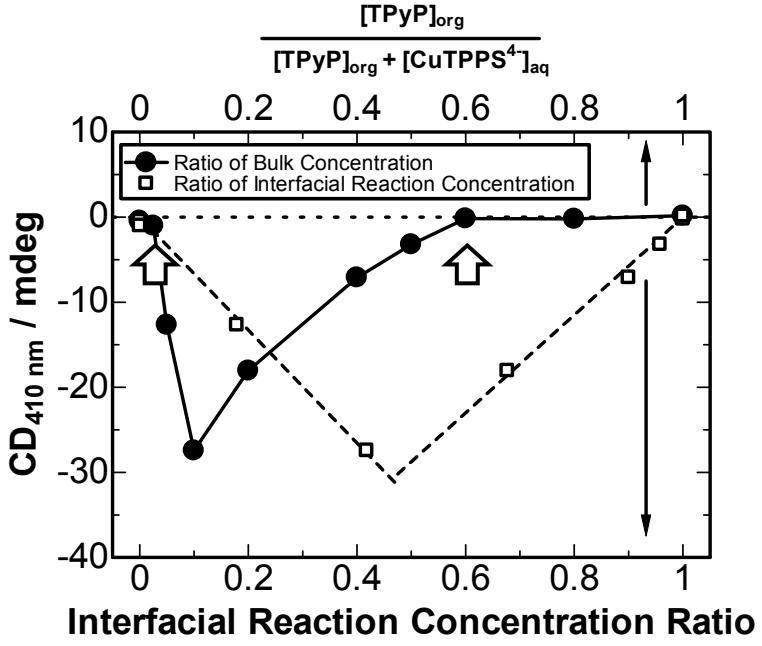

Figure 4. Job plot of H_4TPyP^{4+}-$CuTPPS^{4-}$ hetero-aggregate measured by CLM-CD. $[TPyP]_{org}$ + $[CuTPPS^{4-}]_{aq}$ = 8.0 × 10^{-5} M, $[D\text{-Phe}]_{aq}$ = 9.6 × 10^{-3} M, $[HClO_4]_{aq}$ + $[NaClO_4]_{aq}$ = 0.1 M, pH 2.3, Toluene:Chloroform = 96:4, v/v, t = 30 min. Interfacial reaction concentration ratios were calculated by Eq. (3). Linear dashed lines were fitted lines of interfacial reaction concentration ratio data. The open arrows show the critical concentrations which generate the aggregation.

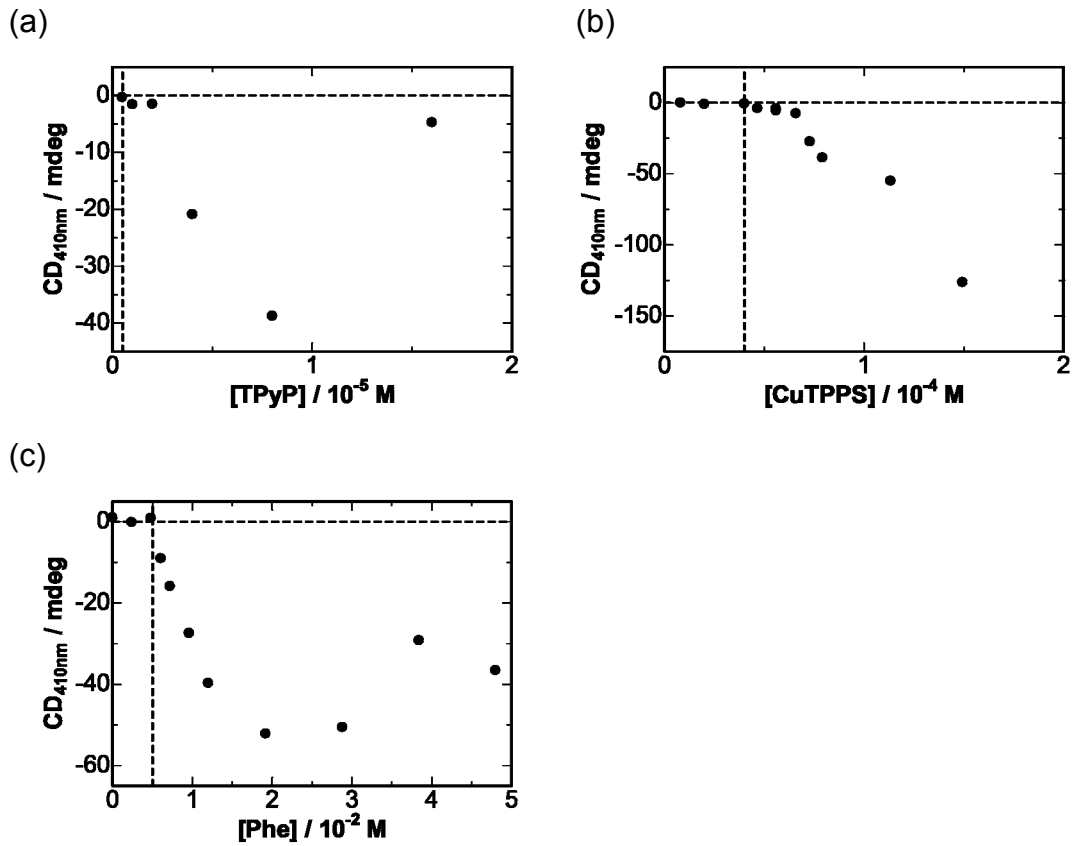

Figure 5. Concentration dependence of CD intensity of TPyP-CuTPPS hetero-aggregates. The dashed lines show critical concentration of each samples. (a) $[TPyP]_{org}$ = 5.0 × 10^{-7} – 1.6 × 10^{-5} M, $[CuTPPS]_{aq}$ = 8.0 × 10^{-5} M, $[D\text{-Phe}]_{aq}$ = 9.6 × 10^{-3} M, $[HClO_4]_{aq}$ + $[NaClO_4]_{aq}$ = 0.1 M, pH 2.3, toluene:chloroform = 96:4, v/v, t = 30 min. (b) $[TPyP]_{org}$ = 8.0 × 10^{-6} M, $[CuTPPS]_{aq}$ = 8.0 × 10^{-6} – 1.6 × 10^{-4} M, $[D\text{-Phe}]_{aq}$ = 9.6 × 10^{-3} M, $[HClO_4]_{aq}$ + $[NaClO_4]_{aq}$ = 0.1 M, pH 2.3, toluene:chloroform = 96:4, v/v, t = 30 min. (c) $[TPyP]_{org}$ = 8.0 × 10^{-6} M, $[CuTPPS]_{aq}$ = 7.2 × 10^{-5} M, $[D\text{-Phe}]_{aq}$ = 0 - 4.8 × 10^{-2} M, $[HClO_4]_{aq}$ + $[NaClO_4]_{aq}$ = 0.1 M, pH 2.3, toluene:chloroform = 96:4, v/v, t = 30 min.

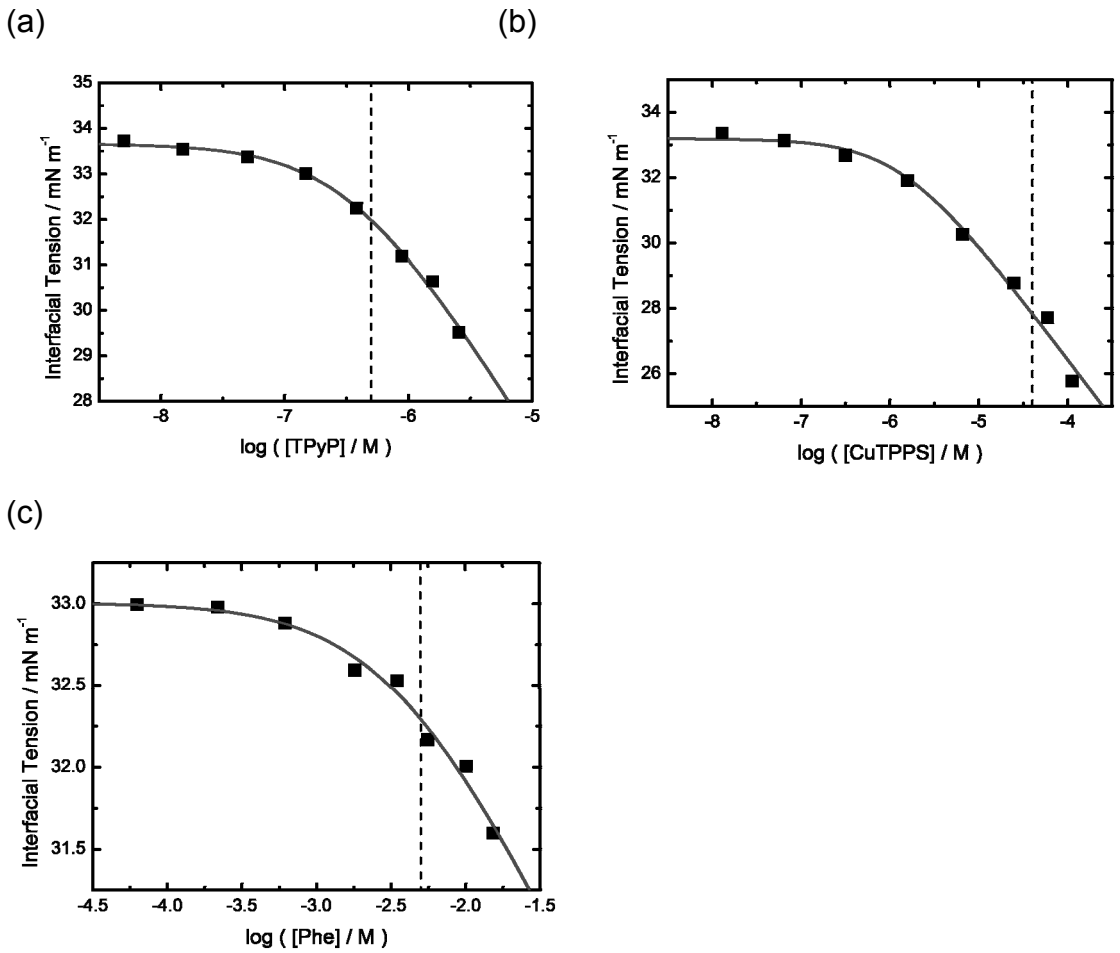

Figure 6. Interfacial tension of phenyalanine measurements by Wilhelmy method. The solid lines are fitted lines by Eq. (1). The dashed lines show critical concentration of each samples. [$HClO_4$] + [$NaClO_4$] = 0.1 M, pH 2.3, toluene:chloroform = 96:4, v/v.

Table 1. Summary of liquid-liquid interfacial adsorption constants, *K'*, and critical concentration of TPyP(org), H_4TPyP^{4+}(aq), $CuTPPS^{4-}$(aq) and phenylalanine(aq).

Chemical species	*K'* / dm	Critical Concentrtion / M
TPyP (org)	5.0×10^{-5}, [a, 9]	5×10^{-7}
H_4TPyP^{4+} (aq)	2.2×10^{-2}, [b]	
$CuTPPS^{4-}$ (aq)	4.6×10^{-3}, [b]	4×10^{-5}
Phe (aq)	9.1×10^{-7}, [b]	5×10^{-3}

[a] Measured by the high-speed stirring method,[9] [$NaClO_4$] = 0.1 M, pH 5.5, toluene:chloroform = 95:5, v/v. [b] Measured by the Wilhelmy balance technique, [$HClO_4$] + [$NaClO_4$] = 0.1 M, pH 2.3, toluene:chloroform = 96:4, v/v.

Composition of TPyP-CuTPPS Hetero-Aggregates in the Toluene/Water System.

The CD spectra of the hetero-aggregate formed at the interface were different from those in the aqueous solution,[4] suggesting the difference in the chiral structure. In addition, Purrello *et al.* reported that H_4TPyP^{4+} and $CuTPPS^{4-}$ reacted 1:1 in aqueous solution.[4] From the circle plots of Figure 5, the largest CD intensity of hetero-aggregates at the interface was apparently observed at 1:9 for the initial concentration ratio of TPyP and $CuTPPS^{4-}$ in the toluene/water system.

To simplify the analysis, we supposed that the bulk concentration exceeding the critical bulk concentration can participate to the formation of the chiral interfacial aggregate, then the product of the interfacial adsorption constants and the bulk excess concentration corresponds to the liquid-liquid interfacial reaction concentration (Eq. (3)). Then, the interfacial reaction concentration ratio was defined by

$$\frac{K_1'([\mathrm{TPyP}]_{\mathrm{org}} - [\mathrm{TPyP}]_{\mathrm{c}})}{K_1'([\mathrm{TPyP}]_{\mathrm{org}} - [\mathrm{TPyP}]_{\mathrm{c}}) + K_2'([\mathrm{CuTPPS}^{4-}]_{\mathrm{aq}} - [\mathrm{CuTPPS}^{4-}]_{\mathrm{c}})} \qquad (3),$$

where K_1' and K_2' are the interfacial adsorption constants of H_4TPyP^{4+} and $CuTPPS^{4-}$, respectively. $[TPyP]_c$ and $[CuTPPS^{4-}]_c$ are the critical bulk concentration of TPyP and $CuTPPS^{4-}$ in the solutions, respectively. Job plot by using the interfacial reaction concentration ratio was also shown with square plots in Figure 5. When the interfacial reaction concentration ratio of H_4TPyP^{4+}:$CuTPPS^{4-}$ was around 1:1, the CD intensity became maximum. This ratio was same with the reaction ratio in the aqueous solution.[4] However, the reported CD spectrum of the aqueous hetero-aggregates showed maxima at ca. 380 nm and 450 nm,[4] which were different from ca. 400 nm, 410 nm and 450 nm of the interfacial hetero-aggregates. Both absorption spectra suggested H-aggregate structure, but the CD spectra suggested different position of positively charged Phe in the aggregate. In the aqueous solution, a positive Phe will associate with H_4TPyP^{4+}-$CuTPPS^{4-}$ complex by hydrophobic interaction with phenyl group. However, at the interface it might be possible that a positive Phe ion will interact with electrostatic interaction to the complex orienting the phenyl group outside, since the liquid-liquid has a lower dielectric constant than the aqueous phase.[11] At the interface, perchlorate ion may behave as a counter ion for the positive Phe ion. Eventually, the distance between the asymmetric carbon in Phe and the chromophre of the porphyrins will be different between the hetero-aggregates formed in the aqueous solution and at the interface.

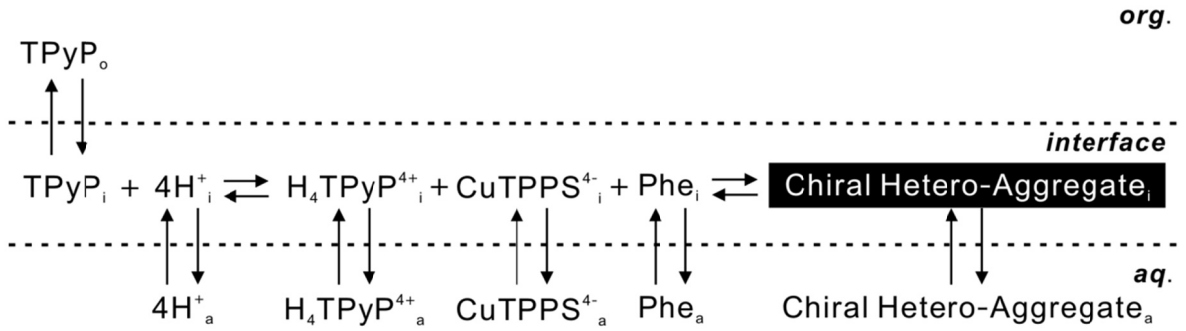

Figure 7. Possible interfacial chiral aggregation scheme.

Conclusion

The hetero-aggregates of H_4TPyP^{4+} and $CuTPPS^{4-}$ showed CD signal corresponded to the chirality of amino acids. The CD signal was true chiral signal not artifact come from optical anisotropy. H_4TPyP^{4+} and $CuTPPS^{4-}$ are working synergistically for the chiral recognition of amino acids. The CD spectra of the hetero-aggregate formed at the interface were different from those in the aqueous solution,[4] suggesting the difference in the chiral structure. Some researcher reported that the structure of chiral aggregates was changed by solvent effect.[12, 13] We demonstrated that the structure of chiral aggregates was also changed by the liquid-liquid interfacial effect.

The hetero-aggregates of H_4TPyP^{4+} and $CuTPPS^{4-}$ could also recognize the chirality of other amino-acids like tyrosine (Tyr) and tryptophan (Trp) at the toluene/water interface, though the CD intensity was smaller than that of Phe hetero-aggregate. Either H_4TPyP^{4+} and $CuTPPS^{4-}$ could not form interfacial aggregate and not recognize the chirality of the amino acid, so it was concluded that H_4TPyP^{4+} and $CuTPPS^{4-}$ are working synergistically for the chiral recognition of amino-acids. There is a possibility that the H_4TPyP^{4+}-$CuTPPS^{4-}$ hetero-aggregate at the liquid-liquid interface can be used for the chiral recognition of various kinds of chiral molecules adsorbable at the liquid-liquid interface, especially for the compounds having no chromophore like alchohols, amines and carboxylic acids. Also, it can be concluded that the present CLM-CD method is a promising tool to investigate the chiral structure and chiral function of hetero-aggregates of porphyrins formed at the liquid-liquid interface.

References

[1] K. Adachi, K. Chayama, H. Watarai, *Langmuir*, **22**, 1630 (2006).

[2] H. Watarai, S. Wada, K. Fujiwara, *Tsinghua Science and Technology*, **11**, 228 (2006).

[3] K. Fujiwara, H. Monjushiro, H. Watarai, *Chem. Phys. Lett.*, **394**, 349 (2004).

[4] L. Rosaria, A. D'urso, A. Mammana, R. Purrello, *Chirality*, **20**, 411 (2008).

[5] H. Nagatani, H. Watarai, *Anal. Chem*., **70**, 2860 (1998).

[6] S. Wada, K. Fujiwara, H. Monjushiro, H. Watarai, *Anal. Sci.*, **20**, 1489 (2004).

[7] H. Takechi, K. Adachi, H. Monjushiro, H. Watarai, *Langmuir*, **24**, 4722 (2008).

[8] K. Adachi, K. Chayama, H. Watarai, *Chirality*, **18**, 599 (2006).

[9] H. Takechi, H. Watarai., *Solv. Extr. Res, Dev. Jpn.*, **14**, 133 (2007).

[10] H. Watarai, F. Funaki, *Langmuir*, **12**, 6717 (1996).

[11] A. Ohashi, H. Watarai, *Langmuir*, **18**, 10292 (2002).

[12] J. Ma, H. S. Cheon, Y. Kishi, *Org. Lett.*, **9**, 319 (2007)**.**

[13] K. Jyothish, M. Hariharan, D. Ramaiah, *Chem. Eur. J.*, **13**, 5944 (2007).

Measurement of Liquid-Liquid Interfacial Aggregates by Transmission Mueller Matrix Ellipsometry

Abstract

Using a conventional circular dichroism spectropolarimeter, CD spectra have been measured not only for the isotropic samples, but also for various anisotropic samples. It is necessary to give a lot of care to such chiral artifacts in CD measurements, unless the samples are completely random-orientation systems such as solutions. The Mueller matrix description contains all the information about the polarization properties of a sample, and measurements of the complete Mueller matrix can be used to investigate the optical activity of the sample. We have measured the linear and circular dichroisms and the linear and circular birefringences of the liquid-liquid interfacial aggregates, which were calculated by the inversion of the Mueller-Jones matrices. We could measure the true interfacial chiral signal except for the artifacts. This is the first work of the liquid-liquid interfacial optical activity mesurements which applied the Mueller matrix method.

Introduction

Circular birefringence (CB) and circular dichroism (CD) are now widely employed for characterizing and quantifying natural and synthetic chiral systems. Using a conventional circular dichroism spectropolarimeter, CD spectra have been measured not only for the isotropic samples, but also for various anisotropic samples such as solid, liquid crystal, film, membrane, micelles and gel. However, the CD spectra of anisotropic samples were more or less accompanied by artifacts due to the optical anisotropies of the samples, such as linear birefringence (LB) and linear dichroism (LD). Therefore, it is necessary to give a lot of care to such chiral artifacts in CD measurements, unless the samples are completely random-orientation systems such as solutions.[1,2] So, the optical activity measurements of the aggregates at the liquid-liquid interface are also paid attention to the artifacts.[3]

The idea of a Mueller matrix measurement is not new. In 1978, R. M. A. Azzam and P. S. Hauge reported papers about Mueller matrix measurement.[4,5] Recently, transmission Mueller matrix ellipsometry, sometimes also referred as Mueller polarimetry, has been applied to the study of anisotropic samples with the aim to study their optical activity. Interesting systems to study with this methodology correspond to the samples containing oriented molecules[6] or crystals[7-9]. Some years ago, generalized ellipsometry and Mueller matrix ellipsometry were started to be used to measure anisotropic samples that could not be studied with conventional ellipsometry. It seems reasonable to think that the future of polarimetric measurements of optical activity in anisotropic samples will have to consider the Mueller matrix in those days. However, it is rare that Mueller matrix measurement is used for chiral anisotropic sample.[10,11] Because the magnitude of CD and CB signals is usually small. Moreover, in the systems where linear birefringence and/or linear dichroism are also present, they usually hinder the effect of CB and CD as they are larger in the orders of magnitude. In the present study, we have measured optical activity of liquid-liquid interfacial chiral aggregates by Mueller matrix polarimeter combined with the centrifugal liquid membrane method. This is the first report of Mueller matrix measurements of the liquid-liquid interface.

Theoretical Background

Stokes vectors and Mueller Matrix.

The most comprehensive way to depict the changes in light polarization, as it interacts with a sample, is to use the Stokes-Mueller formalism.[12] The Stokes vector is a 4-element vector with real components, which can represent any polarization state of light, and the Mueller matrix is a 4×4 real matrix that describes the changes in light polarization as it interacts with an optical element. Once determined for a sample, this Mueller matrix will allow representing all of the sample's polarization properties. In addition, any depolarization of the light beam from the sample will be reflected in the sample Mueller matrix. The partial or complete determination of the Mueller matrix can be achieved by several different polarization dependent techniques, however, many of the sample Mueller matrix elements are not directly related to individual polarization effects. For example, if a compound is chiral then its associated Mueller matrix elements will be affected by the chirality, this relationship is not simple, because the affected Mueller matrix elements also depend on the linear dichroism (LD) and the linear birefringence (LB) of the sample.[13,14] Measurements of CD and CB of liquid organic compounds are much simpler, since all the linear anisotropies (related to a preferential spatial direction) vanish and only pure circular contributions remain.

In the present work, we will use the Stokes–Mueller description of polarized light propagation to specify the irradiance that reaches the detector of the ellipsometer. We represent the Stokes vector as (s_0, s_1, s_2, s_3) where the components are the Stokes parameters. The order of the parameters is total intensity, x- or y-axis linear polarization, 45° linear polarization and circular polarization.[15] It is interesting to note that this most common order of the parameters was different from that of many reports about Mueller matrix ((s_0, s_2, s_3, s_1) in the present notation) and that special attention should be paid in comparing elements of the Mueller matrix.[1,2,16,17] The notation of other papers brings out a direct correlation between the Stokes parameters and the corresponding Pauli spin matrices that allows deriving in a straightforward manner the general Mueller matrix of a sample having both, linear and circular anisotropies.[18]

For thin specimens that show small mixed anisotropies and that CD and CB signals are smaller than LD and LB signals (as is more often the case in practice), we can ignore second-order terms in the chiral anisotropies as well as quadratic terms which involve both, linear and chiral anisotropies. In this case the general Mueller matrix of the sample reduces to:

$$\mathbf{M} = \begin{pmatrix} m_{00} & m_{01} & m_{02} & m_{03} \\ m_{10} & m_{11} & m_{12} & m_{13} \\ m_{20} & m_{21} & m_{22} & m_{23} \\ m_{30} & m_{31} & m_{32} & m_{33} \end{pmatrix}$$

$$\approx e^{-2k} \begin{pmatrix} 1 & -\mathrm{LD} & -\mathrm{LD}' & \mathrm{CD} \\ +\frac{1}{2}(\mathrm{LD}'^2+\mathrm{LD}^2) & & & +\frac{1}{2}(\mathrm{LB}\,\mathrm{LD}'-\mathrm{LB}'\mathrm{LD}) \\ -\mathrm{LD} & 1 & \mathrm{CB} & \mathrm{LB}' \\ & +\frac{1}{2}(\mathrm{LD}^2-\mathrm{LB}'^2) & +\frac{1}{2}(\mathrm{LB}\,\mathrm{LB}'+\mathrm{LD}\,\mathrm{LD}') & \\ -\mathrm{LD}' & -\mathrm{CB} & 1 & -\mathrm{LB} \\ & +\frac{1}{2}(\mathrm{LB}\,\mathrm{LB}'+\mathrm{LD}\,\mathrm{LD}') & +\frac{1}{2}(\mathrm{LD}'^2-\mathrm{LB}^2) & \\ \mathrm{CD} & -\mathrm{LB}' & \mathrm{LB} & 1 \\ -\frac{1}{2}(\mathrm{LB}\,\mathrm{LD}'-\mathrm{LB}'\mathrm{LD}) & & & +\frac{1}{2}(\mathrm{LB}^2-\mathrm{LB}'^2) \end{pmatrix} \quad (1).$$

Here LD' and LB' are respectively 45° linear dichroism and 45° linear birefringence.[13] The quantities LD, LB, LD', LB', CD and CB have the units of radians and are defined in Table 1.[1,13,17,19] The elements of the antidiagonal (m_{03}, m_{12}, m_{21}, m_{30}**)** are chiral difference.

Table 1. Notations and conventions in anisotropic spectroscopy. [1,13,17,19]

Effect	Phenomenological Symbol	Definition	Relation to experiment
Isotropic amplitude absorption	k	$2\pi\kappa l/\lambda_0$	
Isotropic phase retardation	η	$2\pi n l/\lambda_0$	
(x-y) linear dichroism	LD	$ln\ 10(A_x - A_y)/2$	$ln\ 10\Delta\varepsilon' cl/2$
(x-y) linear birefringence	LB	$2\pi(n_x - n_y)l/\lambda_0$	$2\pi\Delta n' l/\lambda_0$
45 º linear dichroism	LD'	$ln\ 10(A_{45} - A_{135})/2$	$ln\ 10\Delta\varepsilon'' cl/2$
45 º linear birefringence	LB'	$2\pi(n_{45} - n_{135})l/\lambda_0$	$2\pi\Delta n''/\lambda_0$
Circular dichroism	CD	$ln\ 10(A_- - A_+)/2$	$ln\ 10\Delta\varepsilon_{\pm} cl/2$
Circular birefringence	CB	$2\pi(n_- - n_+)l/\lambda_0$	$\pi\alpha/90^o$

A stands for standard absorbance, n for refractive index, l for pathlength through the medium, c for molar concentration, α for optical rotation and λ_o for the vacuum wavelength of light. Subscripts specify the polarization of light as x, y, 45 º to the x-axis, 135 º to the x-axis, circular right (+), or left (-).

Analytic inversion of the Mueller-Jones matrix

The Mueller matrix description contains all the information about the polarization properties of a sample, and measurements of the complete Mueller matrix can be used to investigate the optical activity of the sample. However, when many optical polarization effects are simultaneously occurring in the sample (as is the case of the stirred solutions), the resulting elements of the experimental Mueller matrix may reflect several effects lumped together, and their interpretation is not straightforward. A methodology to extract the individual polarization characteristics is thus needed.

One of the most common methods is polar decomposition.[20] However, this matrix factorization has been shown to be inaccurate when the experimental matrices do not have commuting optical properties,[13] since, in this case, the polarization properties of the original Mueller matrix cannot be found in the factors of the decomposition. In contrast, the pseudopolar decomposition[13] preserves all the polarization properties of the system, and, therefore, it can be confidently used to extract the diattenuation and retardation properties of the sample with important noncommutative optical properties.

The general 4×4 Mueller matrix contains 16 independent parameters, whereas the 2×2 Jones complex matrix contains only eight. These parameters can be obtained from the eight physical measurements which one can make in an optical system with a given light path.[21] The definitions for these eight effects are presented in Table 1. If the optical system represented by the Mueller matrix does not depolarize, only seven out of the 16 elements of the Mueller matrix are independent, because nine nonlinear identities exist among the 16 matrix elements.[22] The number of independent parameters in a Mueller–Jones matrix is seven instead of the eight of a Jones matrix, because Mueller matrices cannot represent absolute phase (η). In the case of normalized Jones or Mueller–Jones matrices, the number of independent parameters is six (CD, CB, LD, LB, LD', and LB'). For convenience we will express the elements of the Jones matrix in polar form:

$$\mathbf{J} = \begin{pmatrix} j_{00} & j_{01} \\ j_{10} & j_{11} \end{pmatrix} = e^{i\theta_{00}} \begin{pmatrix} r_{00} & r_{01}e^{i(\theta_{01}-\theta_{00})} \\ r_{10}e^{i(\theta_{10}-\theta_{00})} & r_{11}e^{i(\theta_{11}-\theta_{00})} \end{pmatrix} \quad (2),$$

The Jones matrix elements, as given in Eq. (2), corresponding to a given Mueller–Jones matrix can be calculated using the following equations:[12]

$$r_{00} = \sqrt{\frac{(m_{00}+m_{01}+m_{10}+m_{11})}{2}} \quad (3),$$

$$r_{01} = \sqrt{\frac{(m_{00}-m_{01}+m_{10}-m_{11})}{2}} \quad (4),$$

$$r_{10} = \sqrt{\frac{(m_{00} + m_{01} - m_{10} - m_{11})}{2}} \quad (5),$$

$$r_{11} = \sqrt{\frac{(m_{00} - m_{01} - m_{10} + m_{11})}{2}} \quad (6),$$

$$e^{i(\theta_{01}-\theta_{00})} = \frac{m_{02} + m_{12} - i(m_{03} + m_{13})}{\sqrt{(m_{00} + m_{10})^2 - (m_{01} + m_{11})^2}} \quad (7),$$

$$e^{i(\theta_{10}-\theta_{00})} = \frac{m_{20} + m_{21} + i(m_{30} + m_{31})}{\sqrt{(m_{00} + m_{01})^2 - (m_{10} + m_{11})^2}} \quad (8),$$

$$e^{i(\theta_{11}-\theta_{00})} = \frac{m_{22} + m_{33} + i(m_{32} - m_{23})}{\sqrt{(m_{00} + m_{11})^2 - (m_{10} + m_{01})^2}} \quad (9),$$

There are no physical restrictions on the values of the Jones matrix elements. The effects of Table 1 are incorporated into the general Jones matrix as[13,21]

$$\mathbf{J} = e^{-i\chi/2}\begin{pmatrix} \cos\frac{\mathrm{T}}{2} - \frac{i\mathrm{L}}{\mathrm{T}}\sin\frac{\mathrm{T}}{2} & \frac{(\mathrm{C} - i\mathrm{L}')}{\mathrm{T}}\sin\frac{\mathrm{T}}{2} \\ -\frac{(\mathrm{C} + i\mathrm{L}')}{\mathrm{T}}\sin\frac{\mathrm{T}}{2} & \cos\frac{\mathrm{T}}{2} + \frac{i\mathrm{L}}{\mathrm{T}}\sin\frac{\mathrm{T}}{2} \end{pmatrix} \quad (10),$$

where $\mathrm{T} = \sqrt{\mathrm{L}^2 + \mathrm{L}'^2 + \mathrm{C}^2}$, $\chi \equiv 2(\eta - ik)$, $\mathrm{L} \equiv \mathrm{LB} - i\mathrm{LD}$, $\mathrm{L}' \equiv \mathrm{LB}' - i\mathrm{LD}'$ and $\mathrm{C} \equiv \mathrm{CB} - i\mathrm{CD}$.

For any Mueller–Jones matrix, Eqs. (3)–(9) can be used to calculate r_{00}, r_{01}, r_{10}, r_{11}, $e^{i(\theta_{01}-\theta_{00})}$, $e^{i(\theta_{10}-\theta_{00})}$ and $e^{i(\theta_{11}-\theta_{00})}$. These factors can be identified with the parameterized general Jones matrix in Eq. (10):

$$\begin{pmatrix} \cos\frac{\mathrm{T}}{2} - \frac{i\mathrm{L}}{\mathrm{T}}\sin\frac{\mathrm{T}}{2} & \frac{(\mathrm{C} - i\mathrm{L}')}{\mathrm{T}}\sin\frac{\mathrm{T}}{2} \\ -\frac{(\mathrm{C} + i\mathrm{L}')}{\mathrm{T}}\sin\frac{\mathrm{T}}{2} & \cos\frac{\mathrm{T}}{2} + \frac{i\mathrm{L}}{\mathrm{T}}\sin\frac{\mathrm{T}}{2} \end{pmatrix} = K\begin{pmatrix} r_{00} & r_{01}e^{i(\theta_{01}-\theta_{00})} \\ r_{10}e^{i(\theta_{10}-\theta_{00})} & r_{11}e^{i(\theta_{11}-\theta_{00})} \end{pmatrix} \quad (11),$$

where K is a complex constant that can be determined combining the matrix elements of Eq. (11) and using the identity $\cos^2 \mathrm{T}/2 + \sin^2 \mathrm{T}/2 = 1$:

$$K = \frac{1}{\sqrt{r_{00}r_{11}e^{i(\theta_{11}-\theta_{00})} - r_{01}r_{10}e^{i(\theta_{01}-\theta_{00})}e^{i(\theta_{10}-\theta_{00})}}} \quad (12),$$

Once K is known, the determination of LB, LB', CB, LD, LD', and CD from Eq. (11) becomes straightforward:

$$\mathrm{LB} = \Re[i\Omega(r_{00} - r_{11}e^{i(\theta_{11}-\theta_{00})})] \quad (13),$$

$$\mathrm{LB}' = \Re[i\Omega(r_{01}e^{i(\theta_{01}-\theta_{00})} + r_{10}e^{i(\theta_{10}-\theta_{00})})] \quad (14),$$

$$CB = \Re[\Omega(r_{01}e^{i(\theta_{01}-\theta_{00})} - r_{10}e^{i(\theta_{10}-\theta_{00})})] \quad (15),$$

$$LD = \Im[i\Omega(r_{00} - r_{11}e^{i(\theta_{11}-\theta_{00})})] \quad (16),$$

$$LD' = \Im[i\Omega(r_{01}e^{i(\theta_{01}-\theta_{00})} + r_{10}e^{i(\theta_{10}-\theta_{00})})] \quad (17),$$

$$CD = \Im[\Omega(r_{01}e^{i(\theta_{01}-\theta_{00})} - r_{10}e^{i(\theta_{10}-\theta_{00})})] \quad (18),$$

where $\Omega = TK/[2\sin(T/2)]$, $T = 2\cos^{-1}[K(r_{00} + r_{11}e^{i(\theta_{11}-\theta_{00})})/2]$, and the symbols $\Re$ and $\Im$ respectively denote the real and imaginary parts.[19,23] Arteaga *et al.* reported that this inversion of Mueller-Jones matrices was better method than the polar decomposition in determining LB, LB', CB, LD, LD', and CD from Mueller matrix.[19,23]

Experimental

Materials.

Λ- and Δ-tris(ethylendiamine)cobalt(III) complex was synthesized by the reported method.[24,25] The optical purity of tris(ethylendiamine)cobalt(III) complex was determined by the molar absorptivity, $\varepsilon_{469.5}$ = 84 mol^{-1} cm^{-1} and $\Delta\varepsilon_{492.5}$ = 1.89 mol^{-1} cm^{-1}.[26] The optical purity of Δ-tris(ethylendiamine)cobalt(III) complex was not high, but it was not problem. This sample was only used for comparing the CD spectra measured by commercial CD spectrometer and Stokes polarlimeter.

Cu(II)- meso-tetra(4-sulfonatophenyl) porphine (CuTPPS) was purchased from Frontier Scientific, Inc. (USA). 5,10,15,20-tetra(4-pyridyl)-21*H*,23*H*-porphine (TPyP) was purchased from Aldrich (USA). 5,10,15,20-tetraphenylporphyrin (TPP), S-(+)-nonanol, sodium perchlorate and perchloric acid were purchased from Sigma-Aldrich (USA). Toluene and chloroform were purchased from Scharlab (Spain). Sulfuric acid was purchased from Merck (USA). D-Phenylalanine (D-Phe) was purchased from Wako (Osaka, Japan). L-Phenylalanine (L-Phe) was purchased from Nacalai Tesque Inc. (Kyoto, Japan) and used as received. Toluene was a poor solvent for TPyP. Therefore, toluene containing 4 % chloroform was used as the organic phase solvent. Chloroform was also used to prepare the stock solution of TPyP.

Mueller Matrix Measured by Poxi-spectra.

At first, we tried to use a commercial Stokes polarimeter (Poxi-spectra, Tokyo Instruments Inc., Japan, Figure 1). The Stokes polarimeter has a quarter waveplate and an analyzer, and the quarter waveplate and the analyzer are rotated several times to determine the

Stokes parameters. Blank Stokes vectors, I_0, and Stokes vectors transmitted a sample, I, were measured by irradiated linear polarized light of the several angles. The relation among I_0, I and the sample Mueller matrix, M, was written as

$$I = M I_0 \qquad (19).$$

Equations (1) and (19) were resolved simultaneously by Solver of Microsoft Excel, and we got CD, CB, LD, LD', LB and LB' spectra.

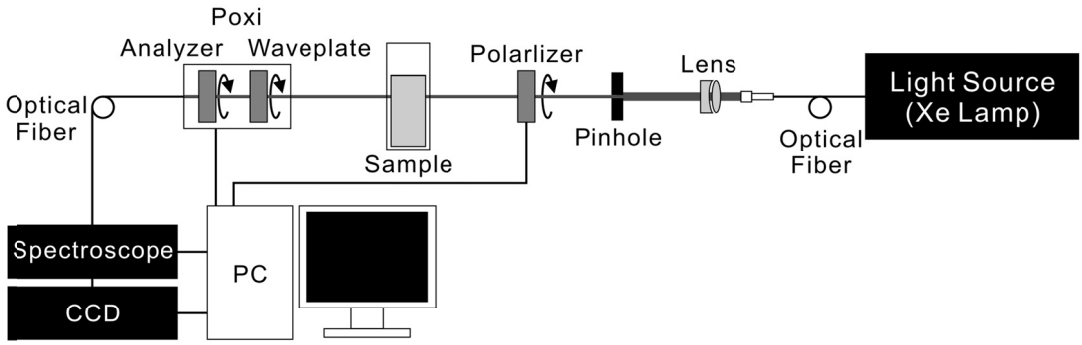

Figure 1. Schematic illustration of the commercial Stokes polarimeter (Poxi-spectra).

Mueller Matrix Measured by Two-Modulator Generalized Ellipsometer.

The instruments of Dual-PEM Stokes polarimeter and the analysis were essentially the same with the one reported previously.[27] The instrument used to measure the Mueller matrices is a two-modulator generalized ellipsometer (2-MGE).[28,29] This instrument uses two polarizer-photoelastic modulator (PEM) pairs,[28] one as a polarization state generator (PSG) and the other as polarization state analyzer (PSA). On a single configuration, this instrument measures 8 independent parameters that correspond to 8 different elements of the Mueller matrix. Complete normalized Mueller matrices are measurable by changing the azimuthal orientations of the PSG and PSA.

Figure 2 displays the basic optical elements that compose the 2-MGE. To detect molecular optical activity, the instrument needs high sensitivity, since typical CB and CD values in molecular optical active samples are around 0.01 rad or lower. This is achieved by using a software-based Fourierlike synchronous detection system, in which the oscillation frequencies of the PEMs as well as some of their multiples or combinations are used as reference signals. The calibration of the instrument is well documented[29] and the calibration parameters of the photoelastic modulators are determined easier than in instruments with a single PEM.

The 2-MGE can be operated in either reflection or transmission mode. In the reflection mode, the 2-MGE can be used, for example, to characterize thin films,[29] as it is one of the

typical applications of ellipsometry; while in the transmission mode[30] (the configuration displayed in Figure 2), it acts as Mueller polarimeter and, among other applications, it can be used to study optical active media.

The formation of interfacial aggregates at the liquid-liquid interface was directly observed using the centrifugal liquid membrane (CLM) methods, described detail in Chapter 2 of this thesis, in which the CLM cell was installed in the 2-MGE. Figure 3 shows the axes of CLM measurements; x axis was horizontal direction, y axis was the perpendicular direction and z axis was the direction of light propagation. 45 º and 135 º directions were the directions where 45 º and 135 ºturned clockwise, looked from a light source, from the x-axis.

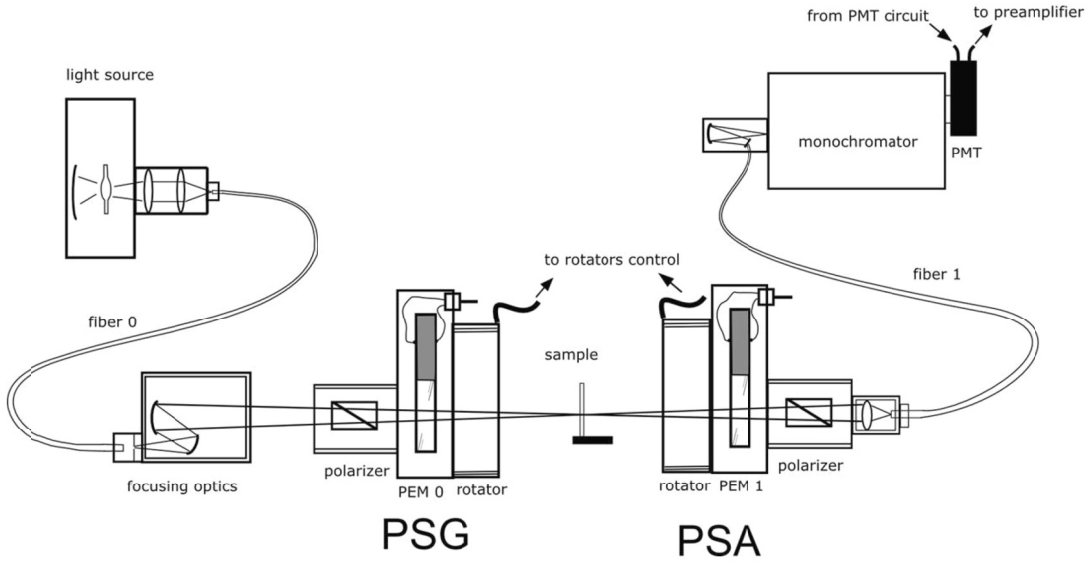

Figure 2. Scheme of the optical setup used in the transmission 2-MGE.[27]

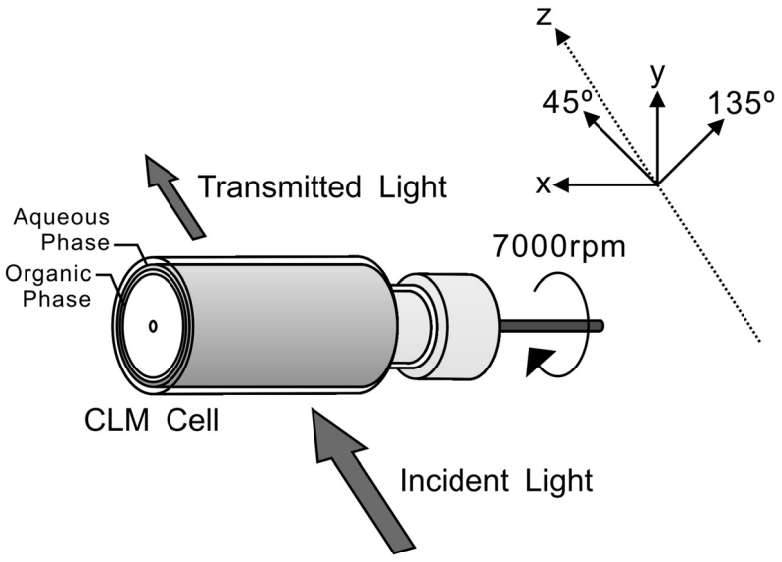

Figure 3. Axes of CLM measurements. x axis was horizontal direction, y axis was the perpendicular direction and z axis was the direction of light propagation. 45 º and 135 º directions were the directions where 45 º and 135 ºturned clockwise, looked from lightsource, from the x-axis.

Results and Discussion

Mueller Matrix Measured by Poxi-spectra.

Figure 3 shows the CD and CB spectra of Λ- and Δ-tris(ethylendiamine)cobalt(III) complex aqueous solution measured by Poxi-spectra, which was expected to have no LD and no LB because of the isotropic sample. The pattern of the CD spectra corresponded to that measured by commercial CD spectrometer. The wavelength dependence of the CB spectra was in the Kramers–Kronig consistency with the measured CD spectra. Thus, Poxi-spectra was found to be able to measure the optical activity of isotropic chiral sample.

But, there were some problems. First, CD spectra measured by Poxi-spectra was noisier than that measured by the commercial CD spectrometer. It is difficult to measure the interfacial chiral aggregates whose CD intensity is very weak (sometimes less than 10 mdeg). Second, when we did not assume that sample was no LD and no LB, we could get the same CD spectra but not CB spectra. We did not use the analytic inversion of the Mueller-Jones matrices. The analysis method was not good. Third, the measurement by Poxi-spectra took long time, ca. 1 hour. CD signal of interfacial chiral aggregates was usually time dependent. Poxi-spectra were difficult to measure the interfacial chiral aggregates. Then, we turned to the 2-MGE and the analytic inversion of the Mueller-Jones matrices.

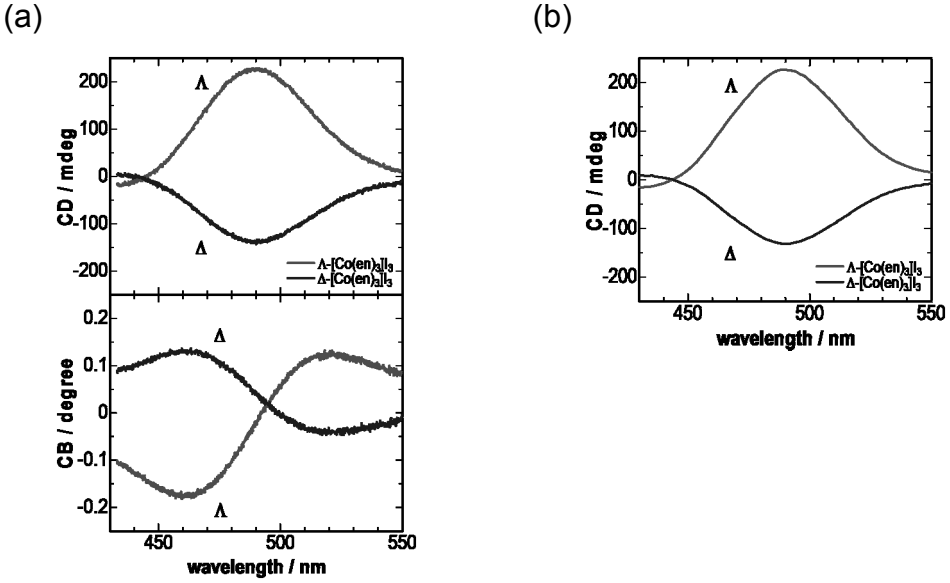

Figure 4. (a) CD and CB spectra of Λ- and Δ-tris(ethylendiamine)cobalt(III) complex aqueous solution in 10 mm cell measured by Poxi-spectra. (b) CD pectra of Λ- and Δ-tris(ethylendiamine)cobalt(III) complex measured by commercial CD spectrometer (J-820E, JASCO, Japan). $[Co(en)_3]I_3$ = 4.0 × 10^{-3} M. e.e.$_\Lambda$ = 91 %, e.e.$_\Delta$ = 54 %.

Mueller Matrix Measured by Two-Modulator Generalized Ellipsometer.

At first, we checked the linear birefringence of the CLM cell by 2-MGE, because commercial CD spectrometer cannot measure linear birefringence. Figure 5 shows the experimentally normalized Mueller matrices of CLM cell. CLM cell had only linear birefringence, m_{23} and m_{32} corresponding to LB, and m_{13} and m_{31} corresponding to LB' , which were larger than other parameters of Mueller matrix. These parameters of Mueller matrix were converted to CD, CB, LD, LB, LD' and LB' by Equations (3)-(9) and Equations (13)-(18). The units of CD, CB, LD, LB, LD' and LB' were converted from radian to milli-degree, because commercial CD spectrometer usually use milli-degree. The converted data was shown in Figure 6. In Figure 6, intensity of the LB in the stagnant CLM cell was much larger than that of LB', and LB sign was negative. So, we can deduce that the fast axis in the CLM cell directed to the rotation axis of the CLM cell and the slow axis directed along the curved wall of the CLM cell. In Figure 6, the intensity of LB in the stagnant CLM cell was smaller than that in the rotation CLM cell. It is guessed that because heterogeneous value of the linear birefringence in the CLM cell were averaged in the high speed rotation CLM cell, and that the measured value of linear birefringence in the high speed rotation CLM cell become smaller than that in the stagnant CLM cell. This phenomenon is advantageous to polarimetry. The linear birefringence of CLM cell was not so serious, and then the CLM cell was no problem to be used for the optical activity measurements.

First liquid-liquid interfacial aggregates sample was TPyP-CuTPPS hetero-aggregates in the toluene-water system. The detail of the aggregates was described in Chapter 3 of this thesis. TPyP-CuTPPS hetero-aggregates in the toluene-water system could recognize the chirality of amino acids. The TPyP-CuTPPS hetero-aggregares recognizing the chirality of the phenylalanine showed CD signals at ca. 400 nm, 410 nm and 450 nm. The hetero-aggregates also had LD signals, but the LD signal intensity was weak. So, the chiral signal of the hetero-aggregates could be measured by commercial CD spectrometer.

Figure 7 shows the Mueller matrix elements of TPyP-CuTPPS hetero-aggregates measured by 2-MGE. These parameters were converted to CD, CB, LD, LB, LD' and LB' by the procedure same as the CLM cell. The results were shown in Figure 8. At first, Mueller matrix of TPyP-CuTPPS hetero-aggregate including D-Phe in Figure 7 was paid to attention. m_{03} and m_{30} including CD signal showed almost same signal. If m_{03} and m_{30} show the opposite sign, these signals are artifacts and not chiral signals. So, TPyP-CuTPPS hetero-aggregate including D-Phe showed chiral signal. TPyP-CuTPPS hetero-aggregate including L-Phe also had chiral signal by same reason. In Figure 8, the CD spectrum of TPyP-CuTPPS hetero-aggregates including D-Phe showed the opposite sign against that including L-Phe.

These spectra were almost same shape with those of Figure 2 in Chapter 3. CB spectra in Figure 8 were in the Kramers–Kronig consistency with the CD spectra. So, the chirality of liquid-liquid interfacial TPyP-CuTPPS hetero-aggregates could be measured by 2-MGE. But CD spectra measured by 2-MGE was noisier than that measured by the commercial CD spectrometer. In addition, the CD intensity was not completely same with the result in Chapter 3, because the sensitivity of a chemical balance used for this experiment was two order lower than that used in Chapter 3, the accuracy of the all solution concentrations were low, and the measurement concentration was not completely the same with that in Chapter 3. Figure 4 (a) in Chapter 3 shows that a slight change of the TPyP concentration gives big influence to CD intensity of TPyP-CuTPPS hetero-aggregates.

The second liquid-liquid interfacial aggregates sample was TPP aggregates in the dodecane-water system. The detail of the aggregate formation was described in Reference [31] and will be published elsewhere. Figure 9 shows CD spectra of TPP aggregates measured by commercial CD spectrometer. The TPP aggregates had large LD. It is thought that the CD spectra of TPP aggregates showed chiral signal, but were affected by the artifacts.

Figure 10 shows the Mueller matrix elements of TPP aggregates including S-(+)-2-nonanol measured by 2-MGE. Figure 11 depicts CD, CB, LD, LB, LD' and LB' obtained as a result of the Mueller-Jones matrices inversion of the experimental matrices shown in Figure 10. TPP aggregates had very large LD and LB signal. Intensity of the LD was much larger than that of LD', and LD sign was negative. So, we can deduce that the axis of TPP aggregates in the CLM cell directed along the curved wall of the CLM cell. CD spectrum in Figure 11 was same sign with that of TPP aggregates including S-(+)-2-nonanol in Figure 9. But CD spectrum shape in Figure 11 was not completely same with that in Figure 9. We think CD spectrum in Figure 11 was true CD spectral shape, because the CD spectrum was obtained after removing the linear contribution. Here, we don't show the detail data in this thesis, but it would be concluded that it is difficult to measure a chiral signal in a sample having large linear contribution. But, it is true that TPP aggregates became chiral at the liquid-liquid interface, because TPP aggregates showed large chiral signal in Figure 11.

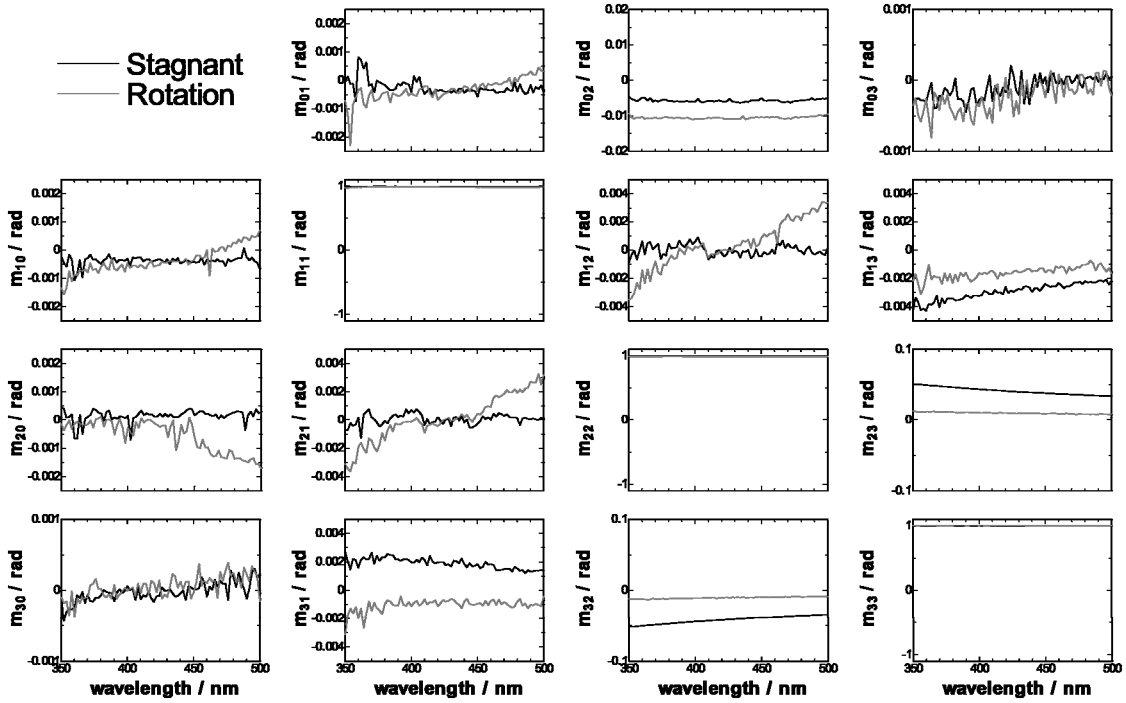

Figure 5. Detail of the experimental normalized Mueller matrices of CLM cell.

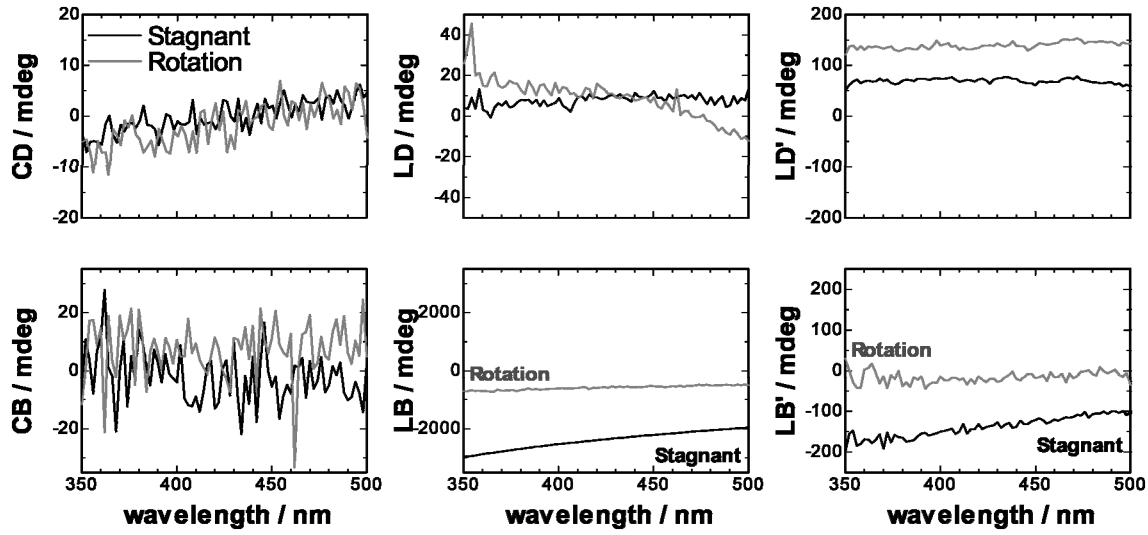

Figure 6. Circular and linear birefringences and dichroisms of an empty CLM cell obtained from the inversion of the Mueller-Jones matrices.

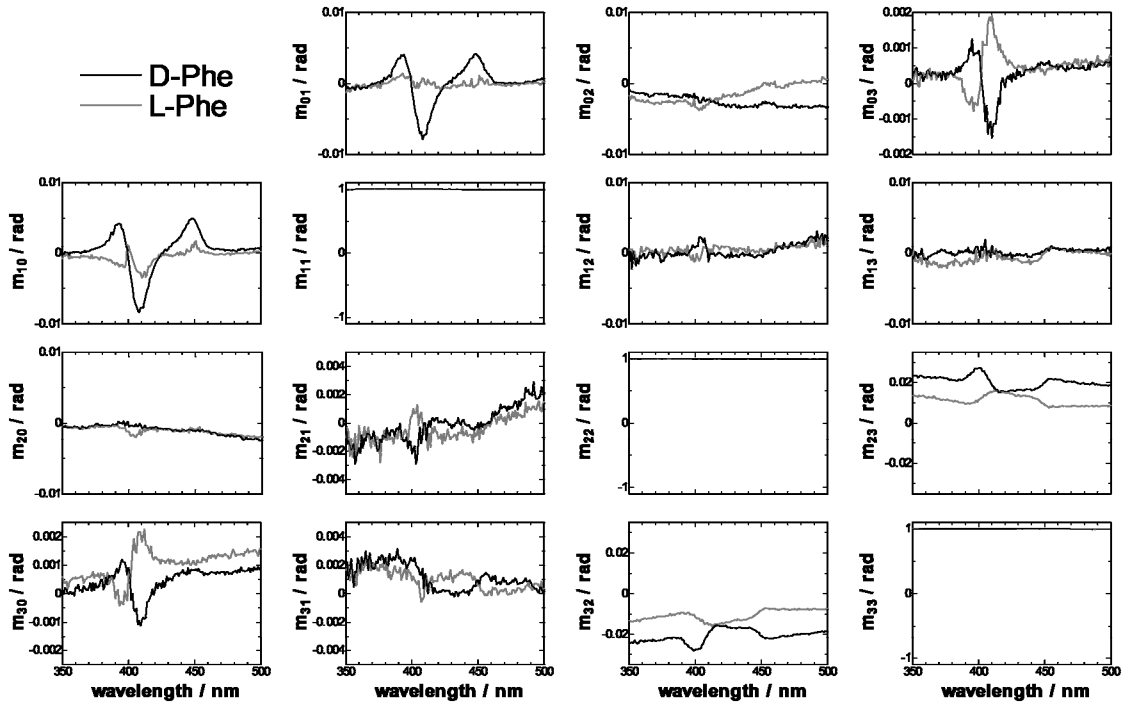

Figure 7. Detail of the experimental normalized Mueller matrices of TPyP-CuTPPS hetero-aggregates in the toluene-water system. $[TPyP]_{org}$ = 8 × 10^{-6} M, $[CuTPPS]_{aq}$ = 1.6 × 10^{-4} M, $[Phe]_{aq}$ = 9.6 × 10^{-3} M, $[HClO_4]_{aq}$ + $[NaClO_4]_{aq}$ = 0.1 M, pH 2.3, toluene:chloroform = 96:4, v/v, t = 30 min.

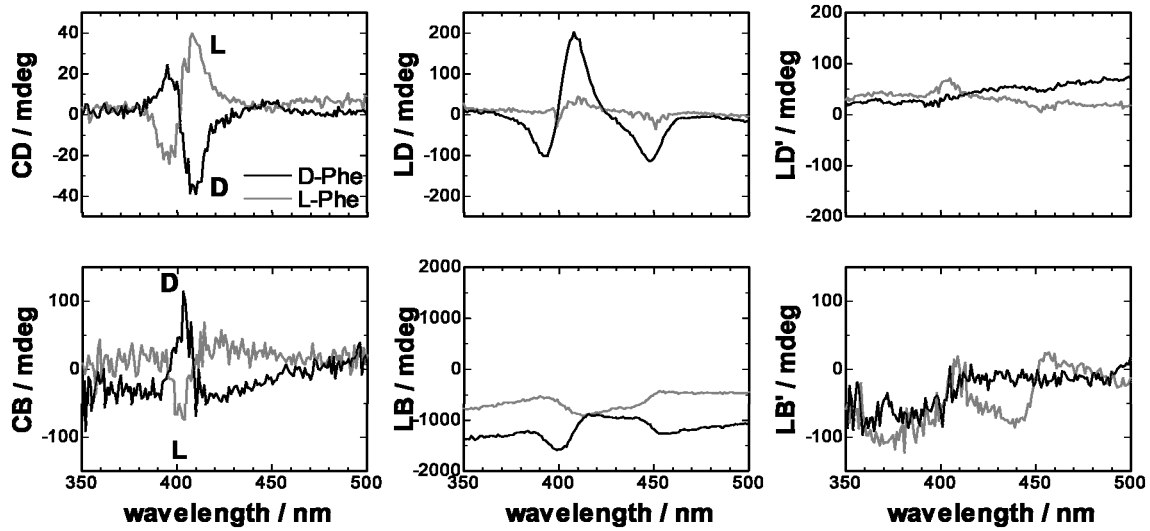

Figure 8. Circular and linear birefringences and dichroisms of TPyP-CuTPPS hetero-aggregates obtained from the inversion of the Mueller-Jones matrices. D-$[TPyP]_{org}$ = 8 × 10^{-6} M, $[CuTPPS]_{aq}$ = 1.6 × 10^{-4} M, $[Phe]_{aq}$ = 9.6 × 10^{-3} M, $[HClO_4]_{aq}$ + $[NaClO_4]_{aq}$ = 0.1 M, pH 2.3, toluene:chloroform = 96:4, v/v, t = 30 min.

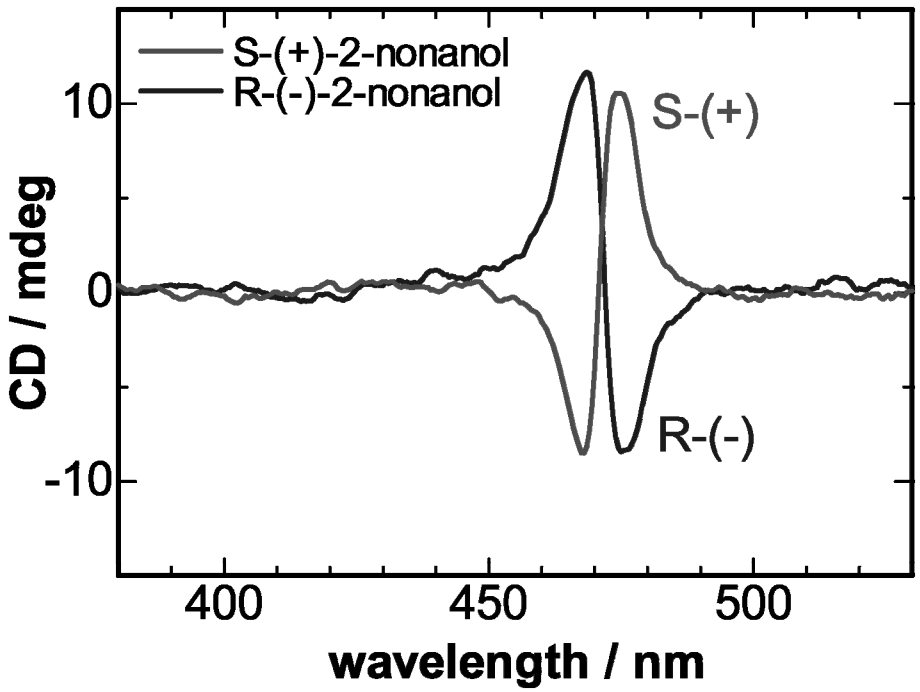

Figure 9. CD spectra of TPP aggregates recognizing the chirality of nonanol. These spectra were measured by commercial CD spectrameter. $[TPP]_{org}$ = 5.7 × 10^{-5} M, $[2\text{-nonanol}]_{org}$ = 1.0 × 10^{-2} M, $[H_2SO_4]_{aq}$ = 4 M, t = 1 min.

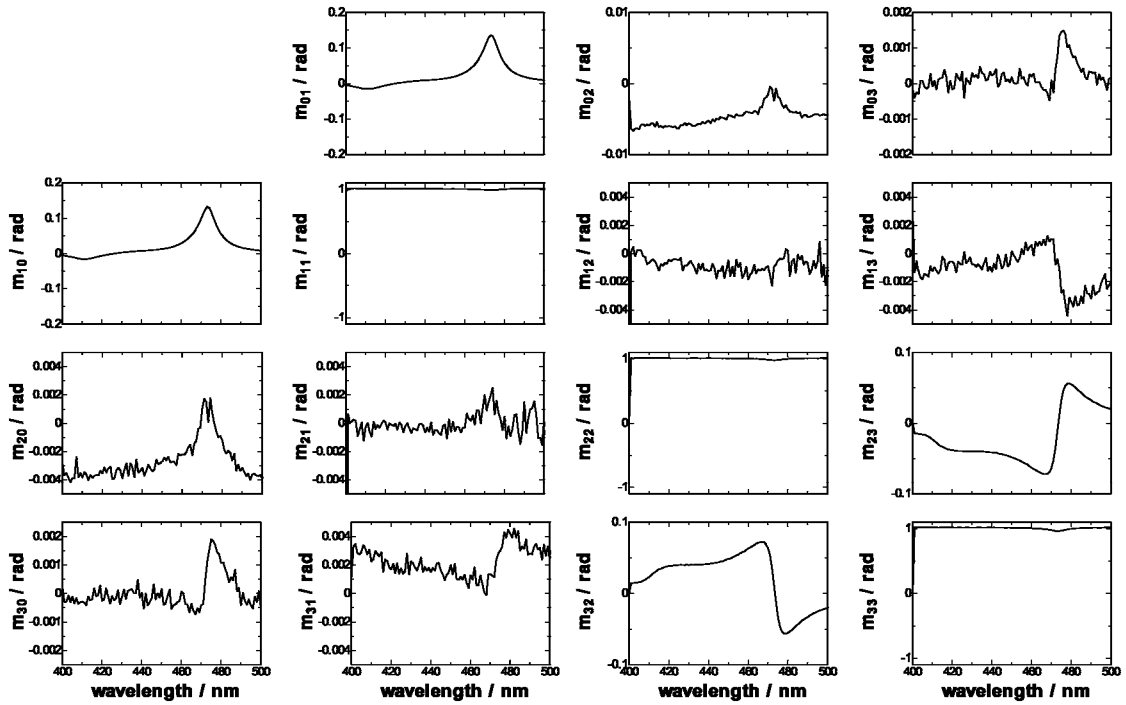

Figure 10. Detail of the experimental normalized Mueller matrices of TPP aggregates including S-(+)-2-nonanol in the dodecane-water system. $[TPP]_{org}$ = 6 × 10^{-5} M, $[S\text{-}(+)\text{-}2\text{-}nonanol]_{org}$ = 5 × 10^{-3} M, $[H_2SO_4]_{aq}$ = 4 M, t = 30 min.

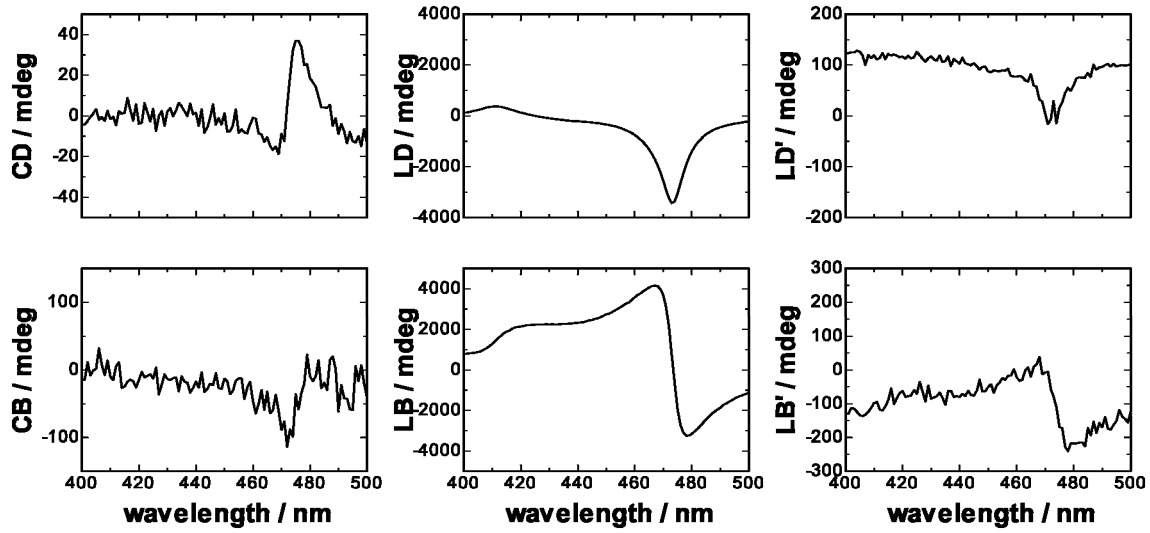

Figure 11. Circular and linear birefringences and dichroisms of TPP aggregates including S-(+)-2-nonanol obtained from the inversion of the Mueller-Jones matrices. $[TPP]_{org}$ = 6 × 10^{-5} M, $[S\text{-}(+)\text{-}2\text{-}nonanol]_{org}$ = 1 × 10^{-2} M, $[H_2SO_4]_{aq}$ = 4 M, t = 30 min.

Conclusions

We measured the Mueller matrices of the liquid-liquid interfacial aggregates. And the linear and circular dichroisms and the linear and circular birefringences of the liquid-liquid interfacial aggregates were calculated by the inversion of the Mueller-Jones matrices. We could measure the true interfacial chiral signal except for the artifacts. It was found that a commercial CD spectrometer has a good sensitivity in the CD measurement but sometimes overlapped by an artifact. On the other hand, Mueller matrix ellipsometer has still less sensitivity, but it can measure the true chiral signal at the liquid-liquid interface. This is the first work of the liquid-liquid interfacial optical activity mesurements by the Mueller matrix method.

References

[1] Y. Shindo, M. Nishio, S. Maeda, *Biopolymers*, **30**, 405 (1990).

[2] R. Kuroda, T. Harada, Y. Shindo, *Rev. Sci. Instrum.*, **72**, 3802 (2001).

[3] H. Takechi, K. Adachi, H. Monjushiro, H. Watarai, *Langmuir*, **24**, 4722 (2008).

[4] R. M. A. Azzam, *Opt. Lett.*, **2**, 148 (1978).

[5] P. S. Hauge, *J. Opt. Soc. Am.*, **68**, 1519 (1978).

[6] O. Arteaga, A. Canillas, R. Purrello, J. M. Ribó, *Opt. Lett.*, **34**, 2177 (2009).

[7] O. Arteaga, A. Canillas, J. Jellison, *Appl. Opt.*, **48**, 5307 (2009).

[8] B. Kahr, J. Freudenthal, E. Gunn, *Acc. Chem. Res.*, **43**, 684 (2010).

[9] J. H. Freudenthal, E. Hollis, B. Kahr, *Chirality*, **21**, S20 (2009).

[10] O. Arteaga, A. Canillas, R. Purrello, J. M. Ribó, *Opt. Lett.*, **34**, 2177 (2009).

[11] O. Arteaga, A. Canillas, J. Crusats, Z. El-Hachemi, J. Llorens, E. Sacristan, J. M. Ribó, *Chem. Phys. Chem.*, **11**, 3511 (2010).

[12] M. Bass *et al.* (Eds.) *Handbook of Optics, Vol. 2*, *2nd ed.* (McGraw-Hill Professional, 1994), Chap. 22.

[13] O. Arteaga, A. Canillas, *J. Opt. Soc. Am. A*, **26**, 783 (2009).

[14] O. Arteaga, A. Canillas, J. Crusats, Z. El-Hachemi, G. E. Jellison Jr., J. Llorca, J. M. Ribó, *Orig. Life Evol. Biosph.*, **40**, 27 (2010).

[15] O. Arteaga, A. Canillas, *J. Opt. Soc. Am. A*, **26**, 783 (2009).

[16] O. Arteaga, Z. El-Hachemi, A. Canillas, *Phys. Stat. Sol. (a)*, **205**, 797 (2008).

[17] H. P. Jensen, J. A. Schelleman, T. Troxell, *Appl. Spectrosc.*, **32**, 192 (1978).

[18] J. Schellman, H. P. Jensen, *Chem. Rev.*, **87**, 1359 (1987).

[19] O. Arteaga, A. Canillas, *Opt. Lett.*, **35**, 559 (2010).

[20] S. Y. Lu, R. A. Chipman, *J. Opt. Soc. Am. A*, **13**, 1106 (1996).

[21] C. R. Jones, *J. Opt. Soc. Am.*, **38**, 671 (1948).

[22] R. Barakat, *Opt. Commun.*, **38**, 159 (1981).

[23] O. Arteaga, A. Canillas, *Opt. Lett.*, **35**, 3525 (2010).

[24] H. S. Booth *et al.* (Eds.) *Inorganic Syntheses, vol. VI*, 183 (1960).

[25] H. S. Booth *et al.* (Eds.) *Inorganic Syntheses, vol. VI*, 186 (1960).

[26] A. J. McCaffery, S. F. Mason, *Mol. Phys.*, **6**, 359 (1963).

[27] O. Arteaga, A. Canillas, *EPJ Web of Conf.*, **5**, 03001 (2010).

[28] G. E. Jellison, F. A. Modine, *Appl. Opt.*, **36**, 8190 (1997).

[29] G. E. Jellison, F. A. Modine, *Appl. Opt.*, **36**, 8184 (1997).

[30] G. E. Jellison, C. O. Griffiths, D. E. Holcomb, C. M. Rouleau, *Appl. Opt.*, **41**, 6555 (2002).

[31] S. Wada, K. Fujiwara, H. Monjushiro, H. Watarai, *J. Phys. Condens. Matter.*, **19,** 375105 (2007).

Concluding Remarks and Outlooks

In this thesis, the validity of chiroptical measurements at the liquid-liquid interface were investigated. Chapter 2 demonstrated that porphyrin aggregates at the liquid-liquid interface showed the false chiroptical signal come from optical anisotropy. The results shows the artifacts from the optical anisotropy cannot be negligible at the liquid-liquid interfacial chiroptical measurements. Chapter 3 showed that we pay attention to the optical anisotropy, the optical activity at the liquid-liquid interface can be measured by commercial CD spectrometer. In Chapter 4, it was shown that the optical activity at the liquid-liquid interface can be calculated by the Mueller matrix measured by the two-modulator generalized ellipsometer. The Mueller matrix description contains all the information about the polarization properties of a medium, we can get both optical activity and optical anisotropy.

True chiroptical measurement method at the liquid-liquid interface was established in this thesis. But, it is still question why achiral molecules become chiral aggregates. I am planning to continue to experiment the chiral aggregates. To understand the basis of this unique form of molecular aggregates and to find ways to synthesize and analyse these nanostructures and functions, the great number of systematic fundamental researches will be required. A synergistic approach, in which chemical, physical and biological approaches are fused together, will offer the best chance of success for developing molecular architecture in the near future.

Acknowledgment

I would like to express my sincere gratitude to Prof. Hitoshi Watarai for his excellent and invaluable guidance throughout my PhD thesis. His keen interest in all my studies has inspired me in many ways. I really enjoyed working on the study and many discussions. I am thankful to him for his constant support and encouragement.

Dr. Takao Fukumoto, and Dr. Masayori Suwa for their helpful suggestions. I wish to thank Prof. Hideaki Monjushiro (High Energy Accelerator Research Organization), Dr. Kenta Adachi (Yamaguchi University) for their advices and encouragements. I would like to thank all member of Watarai laboratory for their constant encouragements throughout my thesis study.

I would like to thank Prof. Josep M. Ribó (University of Barcelona) and Dr. Oriol Arteaga (University of Barcelona) for giving me such opportunity to measure our samples in their laboratory. I am grateful to them for supporting the measurements of Mueller matrix and the analysis.

This thesis was supported a Grant-in-Aid for JSPS Fellows (No. 08J01892).

Hideaki Takechi

February, 2011

Papers Relevant to the Present Study

[1] Linear Dichroism of Zn(II)-Tetrapyridylporphine Aggregates Formed at the Toluene/Water Interface.
Hideaki TAKECHI, Hitoshi WATARAI
Langmuir, **24(9)**, 4722-4728 (2008).

[2] Chiral Analysis of Amino-Acids by Synergistic Hetero-Aggregation with Porphyrins at Liquid-Liquid Interface.
Hideaki TAKECHI, Hitoshi WATARAI
Chem. Lett., **40(3)**, 303-305 (2011).

[3] Chiroptical Measurement of Chiral Aggregates at Liquid-Liquid Interface in Centrifugal Liquid Membrane Cell by Mueller Matrix and Conventional Circular Dichroism Methods.
Hideaki TAKECHI, Oriol ARTEAGA, Josep M. RIBO, Hitoshi WATARAI
Molecules, **16(5)**, 3636-3647 (2011).

Papers Relate to the Present Study

[1] Role of Zn(II) and Pyridyl Groups in the Adsorption and Self-Aggregation of Zinc Tetrapyridylporphine at the Liquid-Liquid Interface.
Hideaki TAKECHI, Hitoshi WATARAI
Solv. Extr. Res. Dev. Jpn., **14**, 133−144 (2007).

[2] Microscopic Measurement of Circular Dichroism Spectra.
Aira MATSUGAKI, Hideaki TAKECHI, Hideaki MONJUSHIRO, Hitoshi WATARAI
Anal. Sci., **24(2)**, 297-300 (2008).

[3] Microscopic Measurement of Second Harmonic Generation from Chiral Surfaces.
Daisuke TOKUNAGA, Hideaki TAKECHI, Jian-Hua YIN, Hitoshi WATARAI, Takahiro OHDE
Anal. Sci., **25(2)**, 311-314 (2009).

[4] Controllable Adsorption and Ideal H-Aggregation Behaviors of Phenothiazine Dyes on the Tungsten Oxide Nanocolloid Surface.
Kenta ADACHI, Tomohiro MITA, Taiki YAMATE, Suzuko YAMAZAKI, Hideaki TAKECHI, Hitoshi WATARAI
Langmuir, **26(1)**, 117-125 (2010).